Contrib Mineral Petrol (1982) 80:160–182

Contributions to Mineralogy and Petrology

Origin of Calc-Alkaline Series Lavas at Medicine Lake Volcano by Fractionation, Assimilation and Mixing

Timothy L. Grove, David C. Gerlach, and Thomas W. Sando
Department of Earth and Planetary Sciences, Massachusetts Institute of Technology, Cambridge, Massachusetts 02139, USA

Abstract. The results of experimental studies and examination of variations in major elements, trace elements and Sr isotopes indicate that fractionation, assimilation and magma mixing combined to produce the lavas at Medicine Lake Highland. Some characteristics of the compositional differences among the members of the calc-alkalic association (basalt-andesite-dacite-rhyolite) can be produced by fractional crystallization, and a fractionation model reproduces the major element trends. Other variations are inconsistent with a fractionation origin. Elevated incompatible element abundances (K and Rb) observed in lavas intermediate between basalt and rhyolite can be produced through assimilation of a crustal component. An accompanying increase in $^{87}Sr/^{86}Sr$ from ~ 0.07030 in basalt to ~ 0.7040 in rhyolite is also consistent with crustal assimilation. The compatible trace element contents (Ni and Sr) of intermediate lavas can not be produced by fractional crystallization, and suggest a magma-mixing origin for some lavas. Unusual phenocryst assemblages and textural criteria in these lavas provide additional evidence for magma mixing.

A phase diagram constructed from the low pressure melting experiments identifies a distributary reaction point, where olivine + augite react to pigeonite. Parental basalts reach this point at low pressures and undergo iron-enrichment at constant SiO_2 content. The resulting liquid line of descent is characteristic of the tholeiitic trend. Calc-alkalic differentiation trends circumvent the distributary reaction point by three processes: fractionation at elevated pH_2O, assimilation and magma mixing.

Introduction

This paper is concerned with the origin of calc-alkaline series lavas at Medicine Lake Highland, California, but the discussions also provide a framework for understanding the petrogenesis of other calc-alkalic series lavas and the origins of the tholeiitic vs. calc-alkalic differentiation trends. The existence of two fractionation trends was not agreed upon by early petrologists. Bowen (1928) concluded that with advancing fractionation basaltic magmas followed a single trend, the calc-alkalic trend, characterized by SiO_2, Na_2O and K_2O enrichment and $FeO + Fe_2O_3$, CaO and MgO depletion. Fenner (1929) disagreed, claiming that the differentiation trend followed in some mafic intrusions was olivine gabbro-gabbro-ferrobasalt. This fractionation trend, the tholeiitic trend, showed $FeO + Fe_2O_3$ enrichment and approximately constant silica as fractionation proceeded. Bowen's view prevailed until Wager and Deer (1939) established the existence of the tholeiitic differentiation trend in the rocks of the Skaergaard layered intrusion. Miyashiro (1974) recognized the existence of continuously variable fractionation trends between these two extremes, and noted that increasing thickness of continental crust above the subduction zone produced a higher proportion of calc-alkalic to tholeiitic series rocks in island-arcs.

The origin of andesite, an intermediate member of the calc-alkalic series, has received much attention. Petrogenetic models for andesite genesis fall into 4 categories: (1) partial melting of hydrated mantle or subducted oceanic crust, (2) fractional crystallization of primary basaltic material; (3) assimilation of a crustal component by parental basaltic magma and (4) mixing of basalt and melted sialic crust. Reviews of these mechanisms for andesite genesis may be found in Green and Ringwood (1968), Boettcher (1973) and Gill (1981).

Kushiro (1972a) suggested that andesitic liquids could be produced through wet melting of lherzolite. The addition of H_2O expands the olivine liquidus volume and allows silica-rich melts to be produced. This suggestion was criticized by other experimental petrologists (Nicholls and Ringwood 1972, 1973; Ringwood 1974; Mysen et al. 1974; Green 1976) who found that liquids produced by melting mantle material under hydrous, high-pressure conditions were dissimilar to andesite, and that reasonable percentages of melting produced tholeiitic liquids. Wet melting of eclogite formed through subduction of oceanic crust has also been proposed as a mechanism for creating liquids of andesitic composition (Yoder and Tilley 1962). Gill (1974) found the trace and rare earth element abundances in andesites were incompatible with the presence of garnet and clinopyroxene as residues left after eclogite partial melting.

Fractional crystallization models have considered the involvement of a variety of phases under a range of physical conditions. Amphibole removal from a mantle-derived melt has been treated by Eggler and Burnham (1973), Allen and Boettcher (1978) and Cawthorn and O'Hara (1976). These experimental studies have delineated amphibole stability over the pressure range 5 to 20 kbar and addressed the conditions of P_{H_2O} necessary for amphibole crystallization. A second proposal is that high f_{O_2} crystallization involving magnetite in crustal magma chambers is a mechanism for producing the calc-alkaline trend from a basaltic precursor

0010-7999/82/0080/0160/$04.60

(Osborn 1959). Gill (1981) concluded that fractional crystallization of the assemblage plagioclase + orthopyroxene/olivine + augite + magnetite is a common process through which andesites are produced.

Some models for andesite genesis have invoked assimilation of a crustal component by a basaltic parent, or mixing of basalt with a rhyolite generated by crustal anatexis. These proposals were based on petrographic observations and the close spatial association of basalt and rhyolite (Larsen et al. 1938; Kuno 1950; Tilley 1950; Waters 1955). Waters and Tilley observed that tholeiitic magmas differentiated in sills to gabbros and ferrogabbros, but similar tholeiite parents were also found to be in close spatial association with andesites and siliceous rocks. To produce the basalt-andesite-dacite-rhyolite association, Waters proposed assimilation of a partial melt of graywacke or argillite. Wilcox (1954) and Bryan (1968) found evidence for assimilation of crustal xenoliths at Paricutin and sucessfully modeled compositional variation among andesites by combined crystallization of olivine + plagioclase and assimilation of crustal xenoliths. The observation of disequilibrium phenocryst assemblages in lavas of intermediate composition (Larsen et al. 1938; Kuno 1950) led to the proposal that some andesites formed by mixing of basalt and rhyolite. Parental basalt was emplaced into and heated the crust, producing rhyolite partial melts. These melts coalesced to form silicic magma chambers, which were injected with rising basaltic melts. Mixing of the basalt and rhyolite produced andesite and intermediate lavas. Eichelberger (1975, 1978) has recently reconsidered this hypothesis for andesite genesis.

Abundant petrographic and field evidence substantiates magma mixing as an important process in the origin of some calc-alkaline lavas. Phenocryst assemblages are found to be out of equilibrium with the bulk rock composition and indicate the mixing of mafic and silicic magmas (Larsen et al. 1938; C.A. Anderson 1941; Kuno 1936, 1950; A.T. Anderson 1976; Eichelberger 1975, 1978). Current interest in physical characteristics of magma chambers (O'Hara 1977; MacBirney 1980; Huppert and Turner 1981) has led to the development of models which predict the existence of compositional zoning and density-stratification, thus allowing the existence of a spectrum of compositions to be present in a single magma chamber and available for mixing.

Though our study is limited to a single Cascade volcano, it provides information on two general petrogenetic problems. First, what processes interact to create the calc-alkalic vs. the tholeiitic trends? Second, how are andesite magmas produced? This paper begins with a summary of the geology of the Medicine Lake volcano, discusses the experimental results and possible fractional crystallization paths for high alumina basalt (HAB) starting compositions. We then compare the major-element, trace-element and isotopic variations observed in the Medicine Lake volcanics and propose a model to explain the observed trends.

Geologic Setting

Stratigraphy and Eruptive History

C.A. Anderson (1941) described the geology of Medicine Lake volcano, and his stratigraphy is used in our discussion. Recent mapping in the volcano has been done by Mertzman (1977a, b, 1979) and Donnelly-Nolan et al. (1981). Reinterpretation of the geology (Donnelly-Nolan, pers. comm.) has enlarged upon and altered Anderson's original stratigraphy. In our discussions we have identified our samples using Anderson's map, and have attempted to relate the major and trace element chemistry taken from Barsky (1975), Condie and Hayslip (1975) and Mertzman (1977a, b, 1979) to Anderson's original stratigraphy.

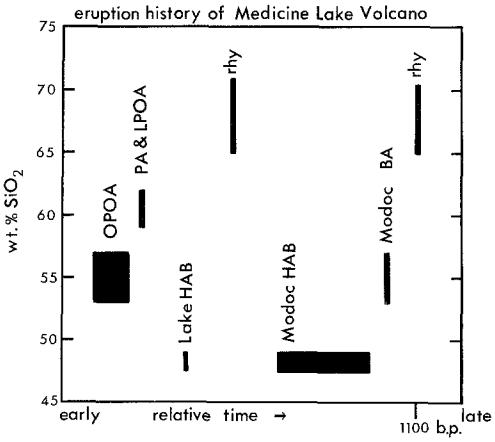

Fig. 1. Composition-surface area-relative time plot for Medicine Lake Highland volcanics. The size of the rectangles represents the surface areas of the lavas and shows compositional variability in terms of wt.% SiO_2 for each extrusive unit. Stratigraphy is from C.A. Anderson (1941). The Warner HAB volcanics which preceded OPOA lavas are not shown on this figure

An eruption history based on Anderson's mapping is summarized in Fig. 1 on a relative time/surface area/composition plot. Extrusion of an unknown volume of Warner high alumina basalt preceded the eruption of the older platy olivine andesites (OPOA). Mertzman (1977a, b) dates the onset of OPOA volcanism at ~900,000 years b.p. The highland grew as a broad shield volcano for an unknown period of time. At the summit of the shield an elliptical arrangement of vents erupted platy andesite (PA), which formed a rampart of andesite volcanoes and terminated the shield-forming event. The eruptive history continued with the extrusion of later platy olivine andesite, (LPOA), Lake HAB, and Mt. Hoffman rhyolite. The latest eruptive cycle began with the extrusion of Modoc intersertal-subophitic high alumina basalt (Modoc HAB) from vents at Mammoth, Giant and Chimney craters on the flanks of the volcanic shield. Flank eruptions of Modoc porphyritic-intergranular basaltic andesite (Modoc BA) followed, forming the Burnt, Paint Pot, Callahan, Schonchin Butte and Devil's Homestead flows. Eruption of rhyolite and mixed dacite at Glass and Little Glass Mountains and at Crater and Medicine Lake flows accompanied extrusion of Modoc basalt in this latest eruptive cycle which terminated ~1,100 years ago (Heiken 1978).

The complete spectrum of calc-alkalic magmas from high alumina basalt to olivine andesite and basaltic andesite, andesite, dacite and rhyolite is present, and proportions are appropriate for fractional crystallization to have produced the observed range of magma types: basalt is the most abundant eruptive type, and rhyolite the least abundant. The order of decreasing volume proportions of lava present at the surface is HAB, BA, andesite, dacite and rhyolite (Fig. 1 and White and McBirney 1978). As in any analysis of this sort, we assume that the lavas represent

liquids. The rocks are generally aphyric, containing less than 5% modal phenocrysts. The dominant phenocrysts in the lavas are olivine, plagioclase, clinopyroxene, and orthopyroxene, allowing phase equilibria at pressures less than 8 kbar (Eggler and Burnham 1973) to be used to model the evolution of the magmatic system. It is possible that high pressure processes played a role in producing the observed compositional spectrum. However, recent geophysical results provide permissive evidence for the existence of a shallow-level magma chamber beneath Medicine Lake volcano (Finn and Williams 1982) at depths <5 km. No evidence for a present-day magma reservoir was found, but a gravity anomaly is consistent with the accumulated residues of fractional crystallization at low pressures (<3 kbar).

Petrographic Characteristics of Lavas

Geologic field relations, phenocryst phase chemistry and textural criteria provide evidence for magma mixing in some basalt, andesite and dacite lavas at Medicine Lake Highland. C.A. Anderson (1941) and Eichelberger (1975, 1980) observed that a single eruptive event at Glass Mountain proceeded from dacite to banded rhyodacite to rhyolite. The bulk composition differences resulted from the mixing of basalt and rhyolite magmas. Phenocrysts are magnesian olivine and augite and calcic plagioclase (bytownite) in intimate association with phenocrysts of andesine and iron-rich orthopyroxene. Similar phenocryst associations were noted in Modoc intergranular BAs. C.A. Anderson (1941, p. 389), speculated, "The most obvious explanation is that these andesine phenocrysts have been picked up from an overlying silicic magma chamber at the time of eruption and that insufficient time elapsed for the reaction of the magma upon the andesine." At Chimney Crater Modoc intersertal HABs containing Fo_{90} olivine and An_{85} plagioclase are interstratified with intergranular basaltic andesites that contain, in addition to the phenocrysts found in the HABs, corroded reverse-zoned phenocrysts of orthopyroxene with iron-rich cores and magnesian rims and plagioclase with andesine cores and labradorite rims (A.T. Anderson 1976; Gerlach and Grove 1982). These extrusive units were produced by basalt-rhyolite magma mixing. Many OPOA, PA and LPOA lavas contain bimodal phenocryst assemblages, and the spread in the liquid's $Mg/(Mg+Fe^{2+})$ and $Ca/(Ca+Na)$ calculated using these phenocrysts indicates that the rock's bulk composition was formed by mixing rhyolite and OPOA. However, other OPOAs lack the disequilibrium phenocryst assemblages found in Modoc BAs and in mixed dacites (Gerlach and Grove 1982).

Experimental Petrology

Selection of Starting Material

Starting materials for the experiments were unaltered lavas that ranged from HAB to andesite (Tables 1, 2). A Modoc intersertal HAB from the E. wall of Giant Crater (79-35g: T42N, R3E, sec 4, 0.40 mi. N. and 0.19 mi. E. of SW corner) was chosen as representative of the parental magmas at the volcano. Two Modoc intergranular BAs were chosen: 79-38b from a railroad cut in the Callahan flow (T44N, R3E, sec. 2, 0.12 mi. S. and 0.19 mi. E. of NW corner) and 187 a sample collected by Smith and Carmichael (1971) from a road cut in the Paint Pot Crater Modoc BA flow. An OPOA (79-20e: T44N, R4E, sec. 18, 0.12 mi. S. and 0.27 mi. E. of NW corner) was sampled from the E. wall of a collapse, and an LPOA (79-9c: T43N, R4E, sec. 8, 0.19 mi. N. and 0.05 mi. E. of SW corner) from the E. wall of a collapse. The compositional range spanned by these starting materials (Table 2) is from 48% SiO_2, 10% MgO and 11% FeO (Modoc HAB) to 59% SiO_2, 3% MgO and 8% FeO (LPOA).

Low pressure melting experiments were performed to determine phase appearance sequence and liquid-lines-of-descent for these Medicine Lake lavas. Cooling rate experiments were also carried out on selected compositions to determine fractional crystallization paths.

Experimental Procedures

Rock chips from fresh hand specimens were used for starting material. Approximately 60 g of chips were reduced to a homogeneous powder in a SPEX shatterbox by grinding for 3 min. The resulting powder was pressed into 10 g discs in an XRF pellet press using elvanol as a binder. These discs were broken into the 25 to 50 mg chips used for each experiment. The chips were sintered on 0.004″ diameter FePt alloy loops that were custommade to be in equilibrium with the silicate charge (Grove 1981) and contained 10 wt.% Fe. The loop and sample were suspended in the hot spots of Deltech DT31VT quenching furnaces in an atmosphere of CO_2/H_2 gas. Temperature was monitored using Pt-Rh10 thermocouples calibrated against the melting points of gold, lithium metasilicate and diopside on the IPTS 1968 temperature scale (Biggar 1972). Oxygen fugacity was monitored using ZrO_2-CaO electrolyte cells, calibrated at the Fe–FeO buffer. The results of the rock melting experiments are presented in Tables 1, 2, 3, 4 and illustrated in Figure 2. The FePt loop technique has minimized Fe loss from the experimental charges, but variable and sometimes significant Na loss has occurred. Approximately 30% Na was lost from the glass 35g-31 and 9c-5 assuming that 2.3 and 4.5 wt.% Na_2O are average for Modoc HAB and LPOA respectively (Mertzman 1977a, b).

Cooling rate experiments (Tables 3, 4) were performed by melting the sample at an initial temperature for the time specified in Table 3. The run was then cooled at a linear rate and terminated at a desired temperature by quenching into water. Cooling rate control was achieved using DT31VT furnaces equipped with Eurotherm 125 temperature programmers wired into the thermocouple circuit. The programmer adds a linear signal to control the temperature drop.

Microprobe Analytical Methods

Compositions of experimentally produced phases were obtained with the MIT 3-spectrometer MAC-5 electron microprobe using on-line data reduction and matrix correction procedures of Bence and Albee (1968) with modifications of Albee and Ray (1970). Silicate glasses, olivines, pigeonites and orthopyroxenes were found to be compositionally homogeneous. Compositionally heterogeneous plagioclases and augites were present even after run times of 600 h in the low T, highly crystalline runs, and indicate that equilibrium was not achieved. When overgrown rims and unreacted cores were present in the run, analyses of the rims are reported in Table 2. A lack of equilibrium was also

Table 1. Run conditions and run products for experiments on Medicine Lake Highland compositions

	Run#	T (°C)	$\log f_{O_2}$	Duration (hours)	Run products[a]	Phase proportions[b]			
79–35g	31	1,234	−7.89	63.7	gl				
	12	1,228	−8.15	97.3	gl, pl, ol	0.93	0.06	0.01	
	11	1,218	−8.27	100.5	gl, pl, ol	0.87	0.09	0.04	
	10	1,210	−8.30	120.2	gl, pl, ol	0.75	0.18	0.07	
	3	1,200	−8.44	144.2	gl, pl, ol	0.71	0.20	0.09	
	1	1,177	−8.80	162.8	gl, pl, ol	0.57	0.29	0.14	
	13	1,166	−8.96	288.1	gl, pl, ol, cpx	0.59	0.26	0.14	0.01[c]
	2	1,160	−8.99	410.0	gl, pl, ol, cpx	0.52	0.32	0.15	0.01[c]
	4	1,153	−9.10	458.1	gl, pl, ol, cpx	0.49	0.30	0.20	0.01[c]
	5	1,137	−9.34	542.5	gl, pl, ol, cpx	0.33	0.43	0.17	0.07[c]
79-38b	3	1,200	−8.44	144.2	gl				
	11	1,185	−8.74	96.2	gl, pl	0.94	0.06		
	1	1,177	−8.80	162.8	gl, pl	0.87	0.13		
	10	1,166	−8.96	288.1	gl, pl, ol	0.77	0.19	0.04	
	2	1,160	−8.99	410.0	gl, pl, ol	0.75	0.21	0.04	
	4	1,153	−9.10	458.1	gl, pl, ol	0.76	0.20	0.04	
	5	1,137	−9.34	542.5	gl, pl, ol, opx	0.60	0.30	0.02	0.08
	6	1,121	−9.54	793.5	gl, pl, ol, opx	0.46	0.38	0.16	0.00
	7	1,106	−9.65	306.8	gl, pl, ol, cpx	0.48	0.40	0.11	0.01
	8	1,089	−9.90	218	gl, pl, cpx	0.32	0.45	0.23	
	9	1,072	−10.16	194.6	gl, pl, cpx, sp	0.26	0.48	0.26	0.00
187	7	1,174	−8.72	129.6	gl, pl, ol				
	12	1,144	−9.22	114.3	gl, pl, ol				
	3	1,135	−9.28	148.7	gl, pl, ol, opx				
	4	1,123	−9.41	164.3	gl, pl, ol, opx				
	5	1,105	−9.71	221.1	gl, pl, ol, cpx				
79-20e	1	1,166	−8.95	143	gl, pl				
	9	1,145	−9.20	113.5	gl, pl, ol	0.82	0.14	0.04	
	4	1,139	−9.29	105.5	gl, pl, ol	0.82	0.13	0.05	
	5	1,130	−9.30	147	gl, pl, ol	0.76	0.17	0.07	
	10	1,116	−9.51	73	gl, pl, ol	0.66	0.28	0.08	
	2	1,106	−9.66	118.5	gl, pl, ol, cpx	0.65	0.11	0.24	0.01[c]
	11	1,099	−9.74	138	gl, pl, ol, cpx				
	8	1,093	−9.94	291	gl, pl, ol, cpx	0.49	0.35	0.05	0.11
	12	1,076	−10.11	330	gl, pl, ol, cpx	0.44	0.37	0.09	0.10
	7	1,059	−10.34	628	gl, pl, cpx, sp				
79-9c	5	1,185	−8.73	96	gl				
	1	1,166	−8.95	143	gl				
	4	1,139	−9.29	105.5	gl, pl	0.92	0.08		
	6	1,130	−9.30	147	gl, pl	0.88	0.12		
	3	1,122	−9.56	140.5	gl, pl	0.89	0.11		
	13	1,116	−9.51	73	gl, pl	0.72	0.28		
	2	1,106	−9.66	118.5	gl, pl, opx	0.82	0.16	0.02	
	11	1,093	−9.94	291	gl, pl, opx, ol	0.64	0.26	0.09	0.01[c]
	7	1,085	−9.95	237.5	gl, pl, opx, ol	0.71	0.23	0.05	0.01[c]
	17	1,076	−10.11	330	gl, pl, opx, sp	0.63	0.30	0.07	0.00
	8	1,059	−10.34	628	gl, pl, cpx, sp	0.52	0.37	0.11	0.00

[a] Abbreviations used: gl = glass, pl = plagioclase, ol = olivine, cpx = clinopyroxene, opx = orthopyroxene, sp = spinel
[b] Weight proportions of phases estimated by linear regression of run compositions
[c] These runs did not come to equilibrium as evidenced by negative values for phase proportions, which were arbitrarily set to 0.01

revealed by large residuals in calculated phase proportions, which were estimated by multiple linear regression (Table 1). Phase compositions obtained by microprobe analysis were assumed to equal the rock composition, allowing calculation of the proportions of phases.

Isotopic Analytical Methods

Sr and Rb analyses were performed on 100-mg splits of rock powders after dissolution in an ultra-pure HF–$HClO_4$–HNO_3 mixture. Separation of Rb and Sr followed a cation exchange method similar to that described by Hart and Brooks (1977). Isotopic analyses were performed on the nine-inch mass spectrometer (NIMA-B) at M.I.T. During analysis, $^{87}Sr/^{86}Sr$ ratios are normalized to 0.1194 for $^{86}Sr/^{88}Sr$ to correct for fractionation. Values of $^{87}Sr/^{86}Sr$ reported here are relative to a 0.7080 for the M.I.T. Eimer and Amend $SrCO_3$ standard.

Table 2. Electron microprobe analyses of run products from Medicine Lake Highland experiments. See table 1 for run conditions and abbreviations

	Run #	Phase	# of Analyses	SiO_2	Al_2O_3	TiO_2	FeO	MnO	MgO	CaO	K_2O	Na_2O	Cr_2O_3	Total
79-35g	31	gl	9	47.5 (7)[a]	18.0 (3)	0.56 (2)	11.1 (2)	0.14 (4)	9.81 (14)	11.4 (1)	0.09 (1)	1.67 (5)	0.02 (2)	100.3
	12	gl	5	47.9 (6)	16.5 (2)	0.72 (3)	10.9 (2)	0.26 (2)	9.92 (17)	11.7 (1)	0.08 (1)	1.35 (7)	0.03 (2)	99.4
		ol	3	39.9 (8)	0.47 (20)	0.01 (1)	14.3 (2)	0.22 (2)	45.9 (4)	0.54 (20)				101.3
		pl	5	46.7 (9)	33.0 (5)		0.63 (8)		0.29 (4)	17.6 (2)	0.03 (1)	1.36 (14)		99.6
	11	gl	5	49.1 (2)	16.6 (3)	0.75 (2)	10.8 (2)	0.11 (2)	9.03 (32)	11.7 (2)	0.06 (1)	1.53 (15)	0.09 (3)	99.8
		ol	4	39.5 (3)	0.37 (18)		15.4 (1)	0.22 (3)	44.2 (6)	0.47 (13)			0.10 (4)	100.3
		pl	4	46.5 (7)	33.2 (4)		0.53 (4)		0.35 (6)	17.3 (2)	0.01 (1)	1.37 (13)		99.3
	10	gl	4	47.4 (5)	15.8 (1)	0.75 (1)	12.6 (2)	0.11 (5)	8.70 (10)	11.4 (8)	0.06 (2)	1.76 (8)	0.08 (4)	98.7
		ol	5	39.5 (2)	0.07 (5)	0.0	17.6 (5)	0.22 (3)	43.3 (5)	0.40 (2)			0.06 (4)	101.2
		pl	3	47.9 (1)	32.2 (3)		0.65 (4)		0.28 (1)	16.1 (1)	0.01 (1)	2.03 (5)		99.2
	3	gl	4	49.5 (7)	15.3 (2)	0.89 (3)	11.5 (1)	0.29 (5)	8.23 (8)	11.6 (1)	0.11 (1)	1.67 (11)	0.07 (2)	99.2
		ol	4	40.1 (2)	0.24 (7)		16.9 (4)	0.23 (4)	43.4 (4)	0.47 (2)				101.3
		pl	3	49.4 (4)	31.4 (3)		0.83 (4)		0.33 (4)	15.7 (1)	0.0	2.42 (4)		100.1
	1	gl	7	49.4 (7)	14.2 (3)	1.05 (2)	12.6 (2)	0.20 (5)	7.39 (27)	12.1 (1)	0.11 (2)	1.76 (10)	0.04 (4)	98.8
		ol	4	38.8 (4)	0.47 (8)		20.7 (2)	0.24 (3)	39.7 (2)	0.72 (12)			0.14 (4)	100.8
		pl	5	47.8 (6)	32.1 (4)		0.84 (9)		0.29 (3)	16.1 (4)	0.01 (1)	2.13 (19)		99.3
	13	gl	5	51.5 (1.2)	14.0 (4)	1.18 (5)	12.0 (2)	0.22 (6)	7.34 (8)	12.1 (2)	0.16 (1)	1.56 (15)	0.05 (1)	100.1
		ol	3	39.4 (5)	0.44 (5)	0.05 (4)	19.9 (1)	0.29 (4)	40.7 (5)	0.57 (5)			0.16 (4)	101.5
		pl	3	48.4 (9)	31.9 (4)		0.72 (10)		0.29 (9)	15.8 (2)	0.03 (1)	2.37 (28)		100.0
		cpx	3	52.7 (1.5)	3.14 (48)	0.70 (38)	8.15 (2.3)	0.23 (11)	15.3 (1.5)	21.0 (5)		0.26 (6)	0.29 (15)	101.7
	2	gl	4	50.7 (7)	13.3 (4)	1.83 (6)	12.5 (4)	0.21 (5)	7.06 (29)	11.5 (1)	0.11 (1)	1.47 (7)	0.01 (1)	98.7
		ol	4	38.9 (2)	0.31 (10)	0.06 (1)	21.1 (1)	0.32 (4)	39.3 (4)	0.51 (5)			0.04 (4)	100.5
		pl	3	48.6 (1)	31.2 (4)		0.84 (20)		0.34 (4)	15.5 (3)	0.03 (1)	2.15 (21)		98.7
		cpx	3	50.1 (6)	2.57 (88)	0.72 (20)	8.95 (39)	0.24 (5)	14.8 (5)	20.5 (3)		0.35 (13)	0.17 (10)	98.5
	4	gl	6	50.5 (3)	13.9 (8)	2.00 (10)	13.1 (4)	0.20 (16)	6.61 (22)	11.7 (2)	0.14 (1)	1.35 (6)	0.09 (4)	96.9
		ol	5	38.4 (4)	0.28 (21)		22.6 (3)	0.25 (3)	38.6 (6)	0.46 (5)			0.0	100.6
		pl	4	48.8 (2)	31.5 (3)		0.66 (9)		0.21 (4)	16.0 (3)	0.01 (1)	2.15 (40)		99.4
		cpx	3	52.1 (7)	2.29 (46)	0.54 (18)	8.15 (40)	0.25 (8)	16.5 (1.2)	20.1 (8)		0.20 (11)	0.27 (9)	100.4
		cpx	3	54.1 (5)	1.43 (45)	0.24 (5)	13.5 (2)	0.37 (5)	25.1 (8)	5.34 (1.5)		0.07 (4)	0.20 (6)	100.3
	5	gl	4	49.4 (5)	12.2 (3)	3.02 (14)	15.5 (1)	0.18 (6)	6.51 (15)	11.2 (1)	0.12 (1)	1.18 (8)	0.04 (3)	99.4
		ol	3	37.6 (7)	0.43 (28)	0.16 (5)	26.3 (5)	0.37 (4)	35.7 (2)	0.60 (19)			0.02 (2)	101.2
		pl	5	47.9 (5)	31.6 (6)		0.91 (13)		0.31 (5)	15.6 (5)	0.07 (1)	2.15 (25)		98.5
		cpx	3	52.4 (8)	2.52 (1.2)	0.55 (17)	10.1 (1.7)	0.21 (7)	17.0 (2.0)	16.3 (3.3)		0.21 (4)	0.29 (4)	99.6
		cpx	3	53.4 (7)	1.57 (72)	0.28 (7)	15.4 (2)	0.32 (3)	23.0 (3)	5.62 (25)		0.12 (12)	0.10 (8)	99.8
79-38b	3	gl	9	54.5 (6)	17.1 (2)	0.86 (2)	8.21 (5)	0.18 (6)	5.85 (4)	8.39 (3)	0.90 (1)	2.65 (36)	0.11 (1)	98.7
	11	gl	5	53.0 (5)	16.6 (1)	0.91 (3)	10.2 (3)	0.21 (2)	5.95 (11)	8.36 (8)	0.93 (2)	2.77 (10)	0.01 (1)	98.9
		pl	4	50.6 (4)	29.7 (3)		0.70 (6)		0.21 (3)	14.8 (2)	0.15 (1)	2.84 (4)		99.0
	1	gl	5	52.5 (3)	15.9 (1)	0.87 (5)	11.7 (2)	0.08 (2)	5.89 (8)	7.91 (9)	0.88 (4)	2.66 (8)	0.0	98.4
		pl	4	50.0 (5)	30.1 (1)		0.87 (8)		0.27 (3)	14.1 (1)	0.15 (2)	2.99 (6)		98.5
	10	gl	6	55.8 (3)	15.1 (2)	1.16 (3)	8.88 (17)	0.19 (3)	5.50 (7)	7.96 (16)	1.10 (3)	2.90 (7)	0.03 (3)	98.6
		ol	4	38.7 (7)	0.31 (31)	0.04 (3)	19.3 (4)	0.32 (3)	41.1 (3)	0.39 (8)			0.03 (2)	100.2
		pl	4	54.0 (1)	27.2 (6)		0.59 (13)		0.24 (3)	11.8 (7)	0.24 (2)	4.08 (22)		98.1

	2	gl	6	57.9 (5)	14.8 (2)	1.16 (3)	8.89 (16)	0.15 (2)	5.64 (5)	7.60 (8)	1.02 (3)	2.04 (35)	0.02 (2)	99.2
		ol	5	39.4 (6)	0.18 (15)	0.0	19.5 (3)	0.31 (5)	41.9 (3)	0.26 (2)			0.08 (4)	101.6
		pl	4	53.7 (1.2)	28.5 (7)		0.81 (7)	0.0	0.31 (6)	12.7 (6)	0.16 (1)	3.77 (27)		99.9
	4	gl	6	56.3 (4)	15.3 (2)	1.12 (5)	10.1 (2)	0.11 (2)	5.58 (12)	7.55 (5)	1.00 (3)	2.29 (9)	0.09 (3)	99.4
		ol	4	38.7 (4)	0.26 (13)		21.3 (2)	0.19 (2)	40.2 (5)	0.29 (3)				100.9
		pl	5	52.0 (6)	28.9 (7)	0.0	0.96 (12)	0.07 (2)	0.29 (9)	13.2 (3)	0.20 (6)	3.52 (18)		99.2
	5	gl	6	56.8 (7)	14.7 (1)	1.53 (8)	10.4 (3)	0.13 (3)	4.66 (18)	7.36 (21)	1.27 (7)	2.26 (14)	0.09	99.2
		ol	3	37.9 (6)	0.23 (5)		24.4 (3)	0.27 (4)	37.6 (6)	0.32 (2)			0.0	100.7
		pl	4	54.7 (6)	28.5 (2)		0.94 (27)		0.34 (10)	12.0 (3)	0.27 (2)	4.08 (17)		100.8
		opx	3	54.5 (7)	1.14 (20)	0.20 (6)	15.2 (4)	0.33 (5)	26.3 (5)	2.28 (14)		0.07 (2)	0.15 (6)	100.2
	6	gl	4	57.8 (7)	13.9 (2)	1.80 (12)	11.0 (4)	0.15 (3)	3.90 (11)	6.93 (12)	1.44 (8)	1.99 (5)	0.09 (4)	99.0
		pl	3	53.4 (2)	28.2 (4)	0.03 (4)	0.75 (13)		0.25 (2)	12.4 (4)	0.24 (2)	3.71 (21)		99.0
		opx	6	53.7 (6)	1.13 (17)	0.12 (2)	17.8 (1)	0.34 (5)	24.3 (3)	2.65 (16)		0.09 (5)	0.10 (4)	100.1
	7	gl	6	56.9 (3)	13.7 (4)	2.08 (8)	11.4 (4)	0.10 (4)	3.54 (8)	7.11 (18)	1.80 (5)	2.31 (29)	0.10 (4)	99.0
		ol	5	36.9 (5)	0.23 (11)		30.7 (3)	0.31 (2)	32.3 (7)	0.39 (4)			0.0	100.8
		pl	5	53.3 (7)	27.5 (3)		1.01 (12)		0.23 (4)	11.8 (3)	0.28 (3)	4.30 (8)		98.4
		cpx	5	53.3 (6)	0.96 (24)	0.34 (7)	17.7 (5)	0.38 (5)	22.7 (8)	4.84 (39)		0.07 (5)	0.08 (5)	100.4
	8	gl	4	58.7 (6)	13.3 (3)	2.56 (19)	10.9 (4)	0.07 (5)	2.43 (9)	5.98 (14)	2.64 (4)	1.97 (19)	0.08 (6)	98.6
		pl	5	54.7 (1.0)	28.7 (3)		0.86 (9)		0.29 (5)	12.2 (3)	0.42 (5)	4.21 (33)		101.4
		cpx	8	52.9 (4)	0.97 (27)	0.49 (9)	18.6 (5)	0.37 (4)	21.8 (3)	4.37 (43)		0.08 (4)	0.10 (3)	99.0
	9	gl	3	61.0 (9)	13.3 (3)	2.74 (17)	9.19 (53)	0.05 (5)	2.56 (23)	5.90 (38)	2.24 (16)	1.42 (33)	0.07 (2)	98.5
		pl	6	54.6 (8)	28.7 (6)		0.86 (8)		0.22 (1)	12.0 (4)	0.48 (5)	4.51 (27)		101.4
		cpx	6	53.3 (3)	0.95 (18)	0.59 (6)	21.3 (2)	0.40 (3)	20.0 (7)	4.88 (48)		0.09 (3)	0.09 (1)	101.6
187	7	gl	5	55.8 (7)	15.8 (2)	1.10 (3)	8.32 (14)	0.11 (4)	6.41 (23)	8.34 (6)	0.82 (4)	2.80 (9)	0.06 (4)	99.6
		ol	5	40.1 (6)	0.46 (6)	0.01 (1)	16.4 (4)	0.24 (4)	44.1 (6)	0.35 (5)			0.15 (6)	101.8
		pl	4	52.4 (6)	29.7 (6)		0.83 (21)		0.44 (10)	13.6 (4)	0.13 (1)	3.62 (16)		100.7
	3	gl	4	57.4 (9)	14.7 (1)	1.55 (8)	9.97 (25)	0.18 (3)	4.71 (11)	8.28 (7)	1.09 (5)	2.32 (33)	0.01 (1)	100.2
		ol	2	38.4 (5)	0.27 (13)	0.13 (9)	22.9 (5)	0.36 (3)	39.0 (9)	0.38 (3)			0.11 (7)	101.5
		pl	3	51.9 (9)	29.9 (5)		0.65 (2)		0.22 (4)	13.4 (5)	0.16 (4)	3.77 (15)		100.0
		cpx	3	55.2 (6)	1.08 (16)	0.31 (6)	14.1 (4)	0.38 (6)	25.3 (7)	4.25 (48)		0.07 (7)	0.13 (2)	100.8
	4	gl	5	58.0 (6)	14.7 (3)	2.00 (7)	9.90 (21)	0.14 (2)	3.99 (11)	7.87 (15)	1.40 (5)	2.64 (11)	0.02 (2)	100.7
		ol	3	38.4 (1)	0.14 (10)	0.12 (1)	25.3 (3)	0.36 (4)	36.7 (6)	0.39 (2)			0.08 (5)	101.5
		pl	3	55.6 (2)	28.3 (5)		0.81 (16)		0.30 (9)	11.6 (2)	0.25 (2)	4.61 (20)		101.5
		cpx	4	54.9 (2)	1.09 (21)	0.38 (10)	14.9 (3)	0.38 (4)	24.6 (7)	4.90 (56)		0.12 (4)	0.15 (3)	101.4
	5	gl	3	57.3 (1)	13.5 (5)	2.75 (4)	10.7 (4)	0.24 (3)	4.06 (45)	7.33 (20)	1.80 (8)	2.59 (30)	0.01 (1)	100.3
		ol	4	37.0 (3)	0.14 (6)	0.06 (3)	28.7 (6)	0.32 (3)	34.3 (6)	0.35 (5)			0.01 (1)	100.9
		pl	5	54.1 (7)	27.6 (9)		1.16 (35)		0.39 (28)	11.5 (6)	0.36 (8)	4.32 (29)		99.4
		cpx	3	52.8 (3)	1.54 (60)	0.60 (26)	16.5 (4)	0.32 (10)	21.8 (1.5)	4.60 (53)		0.41 (25)	0.05 (4)	98.6
79–20e	1	gl	5	54.3 (4)	15.7 (1)	1.21 (5)	10.9 (2)	0.10 (3)	5.71 (8)	7.81 (10)	0.69 (1)	3.00 (11)	0.10 (4)	99.5
		pl	4	54.9 (9)	26.7 (6)		1.00 (5)		0.39 (12)	11.7 (3)	0.18 (2)	4.46 (12)		99.3
	9	gl	7	53.7 (5)	15.4 (1)	1.31 (5)	13.4 (2)	0.15 (3)	5.20 (4)	7.67 (7)	0.74 (2)	3.01 (36)	0.04 (2)	100.6
		pl	6	53.5 (4)	28.8 (7)		0.98 (14)		0.22 (7)	12.0 (2)	0.16 (2)	4.36 (24)		100.0
		ol	8	38.1 (3)	0.12 (3)	0.00 (1)	26.6 (2)	0.27 (2)	35.1 (3)	0.26 (2)			0.00 (1)	100.4

[a] Parenthesized units represent one standard deviation of replicate analyses in terms of least units cited. Thus, 47.5 (7) should be read 47.5 ± 0.7

Table 2 (continued)

	Run#	Phase	# of Anal-yses	SiO_2	Al_2O_3	TiO_2	FeO	MnO	MgO	CaO	K_2O	Na_2O	Cr_2O_3	Total
	4	gl	10	55.1 (7)	14.3 (3)	1.55 (4)	10.9 (2)	0.15 (3)	4.79 (10)	7.86 (15)	0.91 (4)	3.44 (19)	0.04 (4)	99.0
		pl	3	56.3 (1)	26.0 (1)		1.06 (14)		0.40 (10)	10.3 (6)	0.25 (2)	5.31 (24)		99.6
		ol	9	38.0 (4)	0.16 (9)	0.09 (3)	24.0 (2)	0.37 (4)	37.0 (3)	0.37 (3)				100.0
	5	gl	5	55.7 (6)	14.5 (2)	1.69 (6)	11.6 (3)	0.09 (3)	4.41 (7)	7.84 (8)	0.93 (3)	3.29 (15)	0.03 (3)	100.1
		pl	4	54.3 (1)	26.6 (1)		1.07 (10)		0.24 (9)	11.3 (6)	0.19 (2)	4.74 (22)		98.4
		ol	4	37.3 (4)	0.27 (17)	0.08 (1)	26.1 (2)	0.37 (1)	35.2 (4)	0.52 (15)		0.07 (2)		99.9
	10	gl	13	54.5 (6)	13.2 (3)	1.66 (6)	12.9 (3)	0.16 (4)	4.27 (17)	7.84 (3)	0.99 (6)	2.88 (13)	0.04 (3)	98.5
		pl	5	55.1 (8)	27.5 (8)		1.24 (11)		0.29 (7)	11.5 (5)	0.23 (2)	4.61 (18)		100.5
		ol	10	36.8 (4)	0.17 (10)	0.05 (6)	30.0 (6)	0.32 (5)	32.7 (6)	0.44 (5)			0.06 (9)	100.5
	2	gl	4	55.5 (3)	13.5 (3)	2.22 (6)	11.5 (2)	0.19 (4)	3.97 (19)	7.54 (10)	1.16 (2)	2.93 (14)	0.03 (2)	98.6
		pl	5	54.4 (7)	26.6 (4)		1.04 (13)		0.27 (6)	10.6 (2)	0.24 (1)	4.87 (10)		98.4
		ol	6	37.1 (2)	0.14 (8)	0.14 (3)	29.2 (5)	0.45 (3)	32.5 (4)	0.41 (2)				99.9
		cpx	3	53.9 (3)	1.25 (19)	0.35 (8)	17.1 (2)	0.44 (2)	22.8 (4)	4.56 (11)	0.03 (1)	0.25 (10)	0.04 (3)	100.7
	11	gl	9	58.0 (1.3)	13.5 (7)	2.78 (15)	12.8 (4)	0.17 (4)	3.16 (10)	6.85 (17)	1.47 (7)	2.34 (33)	0.07 (3)	101.1
		pl	5	54.7 (7)	27.7 (6)		1.18 (42)		0.28 (13)	11.2 (4)	0.26 (4)	4.84 (15)		100.2
		ol	9	37.3 (1.0)	0.20 (2)	0.07 (4)	30.3 (4)	0.42 (4)	33.9 (4)	0.42 (4)			0.05 (3)	102.6
	8	gl	11	55.1 (4)	12.6 (5)	2.36 (11)	13.4 (6)	0.16 (5)	3.46 (18)	7.42 (20)	1.33 (4)	2.47 (20)	0.02 (2)	98.3
		pl	8	55.1 (7)	26.9 (5)		1.09 (14)		0.27 (8)	10.6 (4)	0.33 (2)	5.20 (29)		99.5
		ol	9	36.2 (5)	0.22 (13)	0.14 (12)	34.4 (3)	0.40 (6)	28.8 (5)	0.47 (9)			0.09 (13)	100.7
		cpx	16	53.3 (4)	0.81 (14)	0.42 (5)	18.8 (4)	0.40 (5)	21.4 (3)	4.50 (18)	0.03 (2)	0.06 (5)	0.12 (4)	99.8
	12	gl	8	57.2 (6)	13.1 (4)	2.71 (13)	13.0 (4)	0.20 (3)	3.11 (30)	6.97 (30)	1.48 (5)	2.11 (19)	0.05 (3)	99.9
		pl	6	56.6 (1.3)	26.8 (1.0)		1.10 (12)		0.23 (4)	10.1 (4)	0.35 (5)	5.38 (17)		100.5
		ol	5	36.8 (9)	0.36 (16)	0.09 (10)	35.8 (6)	0.50 (7)	29.0 (4)	0.43 (5)			0.04 (4)	103.0
		cpx	5	53.2 (1.1)	1.07 (20)	0.43 (12)	19.3 (8)	0.50 (3)	22.1 (1.1)	3.89 (61)	0.02 (2)	0.07 (4)	0.05 (4)	100.6
	7	pl	7	55.9 (7)	25.5 (4)		1.20 (21)		0.09 (6)	9.82 (26)	0.44 (3)	5.22 (14)		98.2
		cpx	4	51.1 (6)	0.95 (15)	0.34 (8)	2.41 (3)	0.41 (2)	17.9 (6)	4.69 (48)	0.03 (2)	0.00	0.02 (2)	99.5
79–9c	5	gl	8	58.9 (4)	16.5 (2)	1.29 (4)	7.91 (20)	0.17 (3)	3.04 (10)	6.08 (14)	1.24 (3)	3.04 (27)	0.00	98.2
	1	gl	4	60.5 (2)	16.3 (1)	1.31 (3)	8.15 (16)	0.07 (2)	2.81 (9)	5.91 (1)	1.33 (3)	2.45 (9)	0.12 (4)	99.0
	4	gl	8	59.5 (6)	15.7 (2)	1.39 (6)	8.68 (40)	0.22 (13)	3.12 (16)	5.67 (24)	1.36 (5)	2.75 (16)	0.01 (1)	98.4
		pl	5	56.4 (1.0)	27.9 (3)		0.89 (9)		0.21 (4)	10.9 (6)	0.24 (3)	5.21 (40)		101.7
	6	gl	9	59.6 (5)	15.6 (1)	1.43 (2)	9.89 (29)	0.15 (4)	3.13 (6)	5.44 (10)	1.36 (3)	2.56 (30)	0.02 (2)	99.2
		pl	5	54.3 (3)	28.6 (1)		1.47 (8)		0.23 (3)	11.1 (2)	0.13 (1)	4.63 (16)		100.4
	3	gl	7	59.7 (7)	15.4 (3)	1.53 (6)	8.78 (52)	0.20 (3)	3.45 (26)	5.62 (15)	1.39 (6)	2.58 (16)	0.00	98.7
		pl	3	56.1 (1.2)	27.6 (8)		0.96 (14)		0.27 (11)	10.8 (8)	0.23 (3)	5.12 (30)		101.0
	13	gl	3	55.7 (4)	14.1 (4)	1.30 (7)	14.0 (3)	0.12 (2)	3.24 (8)	5.69 (12)	1.27 (2)	2.51 (32)	0.03 (3)	98.0
		pl	5	55.9 (8)	27.2 (4)		1.02 (15)		0.14 (4)	10.8 (5)	0.26 (3)	5.62 (21)		100.9
	2	gl	8	60.3 (9)	14.6 (2)	1.58 (7)	9.19 (39)	0.20 (4)	3.17 (12)	5.26 (18)	1.47 (8)	2.33 (16)	0.01 (2)	98.2
		pl	5	55.4 (1.0)	28.3 (5)		0.86 (20)		0.21 (8)	11.1 (2)	0.21 (1)	4.97 (22)		101.0
		opx	6	53.1 (5)	0.91 (24)	0.33 (6)	17.6 (8)	0.49 (12)	24.8 (7)	1.67 (17)	0.03 (1)	0.03 (6)	0.00 (1)	99.0
	11	gl	13	60.5 (6)	13.6 (1)	1.75 (8)	10.6 (4)	0.13 (3)	2.79 (14)	5.15 (19)	1.67 (5)	1.82 (23)	0.02 (2)	98.1
		pl	9	56.0 (8)	26.9 (5)		1.07 (20)		0.18 (6)	10.5 (4)	0.28 (3)	5.17 (24)		100.1
		opx	13	53.1 (4)	0.80 (40)	0.31 (6)	20.3 (6)	0.41 (5)	22.4 (6)	2.90 (23)	0.02 (2)	0.02 (2)	0.03 (4)	99.9
		ol	8	36.2 (5)	0.16 (5)	0.18 (8)	33.6 (6)	0.44 (6)	29.1 (4)	0.33 (3)			0.04 (4)	100.1

Table 2 (continued)

79–9c	7	gl	7	60.8 (5)	13.7 (13)	1.95 (5)	11.3 (1)	0.17 (2)	2.55 (4)	5.01 (13)	1.67 (6)	1.67 (30)	0.01 (1)	98.8
		pl	4	55.3 (6)	27.6 (3)		1.48 (20)		0.16 (5)	10.0 (5)	0.19 (2)	5.17 (18)		99.9
		opx	11	52.3 (3)	0.83 (15)	0.38 (4)	20.9 (6)	0.52 (5)	21.9 (5)	2.78 (27)	0.03 (2)	0.04 (4)	0.05 (4)	99.8
		ol	4	35.8 (7)	0.53 (33)	0.24 (11)	36.5 (1.2)	0.62 (3)	26.4 (4)	0.41 (11)			0.11 (2)	100.6
	17	gl	10	63.2 (1.1)	13.9 (3)	1.84 (8)	9.88 (39)	0.16 (2)	2.37 (16)	4.98 (22)	1.82 (7)	1.47 (24)	0.03 (4)	99.6
		pl	6	57.2 (4)	26.5 (3)		1.12 (30)		0.21 (9)	9.60 (30)	0.40 (1)	5.50 (12)		100.5
		opx	8	53.2 (1.3)	1.19 (15)	0.58 (6)	20.5 (8)	0.52 (6)	22.4 (5)	2.74 (13)	0.05 (1)	0.05 (5)	0.03 (4)	101.2
	8	gl	6	64.1 (2)	13.4 (5)	1.99 (19)	9.33 (11)	0.15 (6)	1.53 (25)	4.44 (27)	2.11 (8)	1.53 (16)	0.01 (1)	98.6
		pl	5	57.3 (4)	26.5 (7)		1.41 (11)		0.13 (5)	9.07 (13)	0.30 (4)	5.70 (27)		100.4
		cpx	15	51.4 (5)	0.86 (14)	0.50 (5)	24.5 (5)	0.54 (5)	18.2 (4)	3.43 (13)	0.06 (3)	0.07 (9)	0.06 (4)	99.6

Table 3. High f_{O_2} and cooling rate experiments on 79-35g and 79-38b

High f_{O_2} experiments

	Run#	T(°C)	log f_{O_2}	Duration (hours)	Run products
79-35g	46	1,195	−6.63	165	gl, pl, ol
	48	1,181	−6.73	100	gl, pl, ol
	40	1,167	−6.81	161	gl, pl, ol
	41	1,147	−7.24	139	gl, pl, ol, px
	44	1,195	−4.53	120.5	gl, pl, ol, sp
	45	1,180	−4.83	121	gl, pl, ol, sp
	42	1,166	−4.80	117	gl, pl, ol, sp, px
	43	1,148	−5.13	117	gl, pl, ol, sp, px

Cooling rate experiments

	Run #	T_{init} duration		f_{O_2}	Cooling rate (°C/hour)	Duration (hours)	T final (°C)	Run products
		(°C)	(hours)					
79-35g	17	1,224	17.5	QFM[a]	2.82	44	1,100	gl, pl, ol
	18	1,224	17.5	QFM	2.98	54	1,063	gl, pl, ol, px
	19	1,223	21	QFM	2.91	69.5	1,021	gl, pl, ol, px, sp
	20	1,223	21	QFM	2.96	81	983	gl, pl, ol, px, sp
	25	1,228	23	NNO+1	2.66	39.5	1,123	gl, pl, ol, px
	26	1,228	23	NNO+1	2.70	61.5	1,062	gl, pl, ol, px, sp
79-38b	12	1,173	14.5	QFM	1.58	190	872	gl, pl, px, sp
	17	1,185	37	QFM	1.31	197.5	927	gl, pl, px, sp
	18	1,173	46	QFM	1.09	146.5	1,014	gl, pl, ol, px, sp

[a] The cooling experiment was begun at the indicated buffer. QFM = quartz-fayalite-magnetite. NNO + 1 indicates 1 order of magnitude above the nickel-nickel oxide buffer

Table 4. Electron microprobe analyses of glasses in high f_{O_2} and selected cooling rate experiments. See Table 3 for run conditions

	Run #	# or Analyses	SiO_2	Al_2O_3	TiO_2	FeO	MnO	MgO	CaO	K_2O	Na_2O	Cr_2O_3	Totals
79–35g	46	9	49.0 (2)	15.4 (2)	0.88 (3)	10.8 (2)	0.22 (3)	8.49 (8)	11.7 (9)	0.15 (1)	2.52 (12)	0.05 (3)	99.2
	48	7	48.3 (4)	14.5 (3)	1.00 (5)	11.6 (2)	0.19 (3)	7.77 (36)	12.0 (2)	0.19 (1)	2.67 (18)	0.04 (3)	98.3
	40	8	49.6 (4)	14.1 (2)	1.21 (6)	11.9 (4)	0.22 (4)	7.30 (15)	12.2 (1)	0.18 (1)	2.68 (10)	0.05 (3)	99.4
	41	7	50.0 (6)	13.5 (7)	1.81 (15)	13.2 (4)	0.25 (3)	6.32 (16)	11.3 (1.5)	0.23 (2)	2.49 (8)	0.02 (2)	99.1
	44	7	47.7 (4)	14.8 (3)	0.89 (5)	11.9 (2)	0.19 (2)	8.61 (16)	11.6 (7)	0.14 (1)	2.42 (7)	0.02 (3)	98.3
	45	8	49.1 (3)	14.3 (5)	0.99 (5)	12.1 (4)	0.21 (4)	8.05 (27)	12.0 (2)	0.17 (1)	2.62 (8)	0.04 (3)	99.6
	42	6	50.4 (4)	13.8 (7)	1.26 (6)	11.2 (3)	0.23 (2)	7.24 (32)	11.2 (2.1)	0.21 (2)	2.82 (12)	0.01 (1)	98.4
	43	3	52.4 (6)	13.3 (5)	1.62 (7)	10.8 (4)	0.23 (2)	6.42 (24)	10.2 (4)	0.32 (3)	2.83 (29)	0.01 (1)	98.1
79–38b	12	3	73.2 (2.1)	12.9 (7)	1.57 (63)	3.97 (1.86)	0.06 (3)	0.19 (4)	1.52 (49)	4.02 (69)	3.95 (1.17)	0.13 (23)	101.5
	17	2	69.1 (1.0)	11.0 (1)	1.40 (6)	6.85 (14)	0.11 (3)	0.29 (7)	1.89 (21)	4.23 (5)	1.31 (9)	0.04 (5)	96.2[a]
		2	39.2 (5)	4.18 (43)	6.75 (19)	30.8 (6)	0.61 (2)	1.96 (4)	8.00 (10)	0.63 (7)	1.20 (9)	0.06 (1)	93.0
	18	4	64.5 (5)	12.1 (3)	2.76 (21)	9.32 (34)	0.13 (4)	1.12 (8)	3.98 (24)	2.85 (5)	1.66 (17)	0.0	98.4
79–35g	17	5	46.9 (5)	10.2 (2)	2.14 (17)	24.2 (4)	0.38 (4)	3.01 (7)	9.85 (13)	0.37 (2)	3.36 (19)	0.01 (2)	99.4
	18	7	47.9 (6)	11.5 (3)	1.67 (10)	19.5 (11)	0.30 (4)	4.31 (44)	11.3 (8)	0.26 (3)	3.06 (14)	0.01 (1)	99.7
	19	6	47.4 (1.1)	8.33 (25)	3.35 (69)	25.7 (10)	0.46 (6)	1.26 (11)	8.38 (31)	0.71 (8)	3.33 (11)	0.01 (2)	100.0
	20	4	55.1 (1.2)	8.95 (68)	1.83 (38)	21.9 (16)	0.43 (13)	0.33 (5)	6.39 (57)	1.34 (13)	2.50 (43)	0.02 (2)	98.7
	25	6	49.1 (4)	11.4 (2)	1.42 (7)	15.1 (2)	0.25 (3)	6.11 (15)	12.6 (1.1)	0.19 (2)	2.67 (14)	0.04 (3)	98.9
	26	3	50.9 (1.1)	10.2 (2)	3.53 (95)	19.3 (5)	0.36 (7)	2.89 (15)	7.51 (6)	0.64 (5)	3.13 (27)	0.02 (2)	98.5

[a] Run 79–38b 17 contains immiscible ferrobasaltic and dacitic liquids

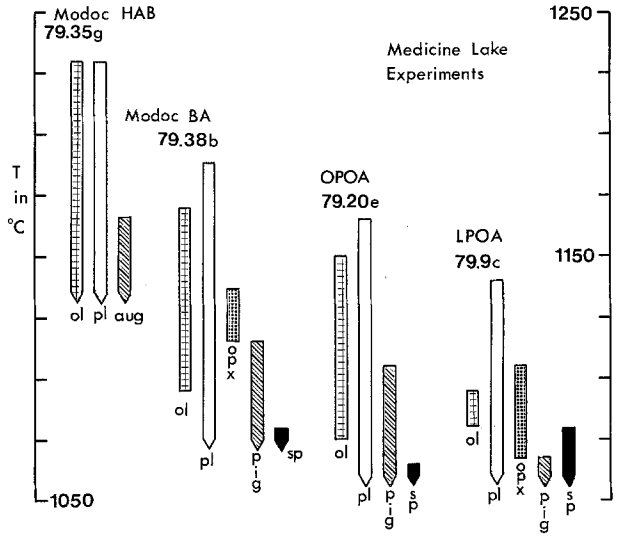

Fig. 2. Results of melting experiments on Medicine Lake Highland compositions. The order of phase appearance in the Modoc BA, OPOA and LPOA preclude a relationship to the HAB by low-P fractional crystallization. Experiments were run at the quartz-fayalite-magnetite (QFM) buffer

Table 5. Isotopic analyses of Medicine Lake Highland rocks

Sample	Rb (ppm)	Sr (ppm)	$^{87}Sr/^{86}Sr$
79-35i (Modoc HAB[a])	1.4	171	0.70340±5
79-40e (Modoc BA)	21.3	207	0.70332±5
80-13 (Modoc BA)	23.4	412	0.70369±5
79-32 (Glass Mtn. rhyolite)	149	112	0.70411±5
80-11 (OPOA)	8.8	375	0.70360±5
79-25a (OPOA)	14.5	641	0.70344±5
79-17 (OPOA)	20.7	616	0.70358±3
79-18 (OPOA)	9.1	379	0.70356±3
79-37j (OPOA)	16.9	599	0.70349±3

[a] Sample localities: 79-35i: same locality as 79-35g. 79-40e: Fleener's Chimney, T45N, R3E, sec 12, 0.25 mi. S. and 0.25 mi. W. of NE corner. 80-13: near Lava Camp, T44N, R3E, sec 3, 0.5 mi. S. and 0.19 mi. E. of NW corner. 79-32: T44N, R4E, sec 26, 0.1 mi. N. and 0.12 mi. E. of SW corner. 80-11: T44N, R3E, sec 14, 0.31 mi. S. and 0.5 mi. E. of NW corner. 79-25a: T44N, R2E, sec 24, 0.13 mi. S. of NW corner. 79-17: T44N, R3E, sec 23, 0.08 mi. S. and 0.47 mi. W. of NE corner. 79-18: T44N, R3E, sec 14, 0.37 mi. S. and 0.44 mi. E. of NW corner. 79-37j: T44N, R3E, sec 8, 0.4 mi. N. and 0.31 mi. W. of SE corner

Liquid Line of Descent at Medicine Lake

In this section we consider the crystallization paths followed by high-alumina basalt starting compositions, and infer the processes that led to the compositional variation observed in the Medicine Lake lavas. The Modoc intersertal-subophitic high alumina basalt (Modoc HAB) is chosen as representative of the parental magma type at the volcano. Though the sample used for the experiments (79-35g) came from one of the youngest flows, HABs of similar bulk compositions have been erupted throughout the volcano's history. The pre-shield HAB units (Anderson's Warner basalt) and later Modoc HABs are high in MgO (8.5 to 10 wt.%) and Al_2O_3 (17 to 21 wt.%) with SiO_2 contents of 47 to

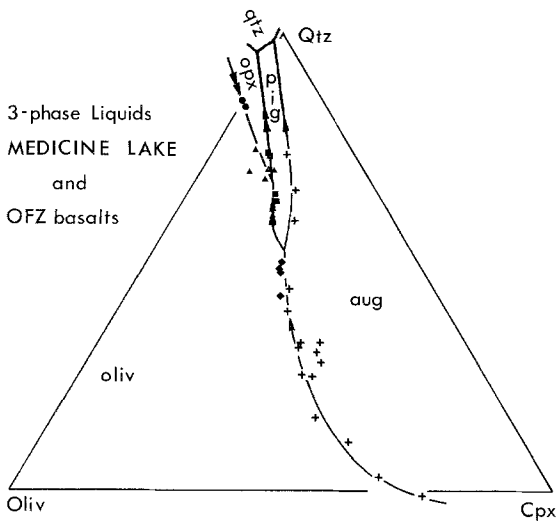

Fig. 3. Low-pressure liquidus for Medicine Lake compositions. Projection is from plagioclase onto plane olivine (*Oliv*)-clinopyroxene (*Cpx*)-silica (*Qtz*). Liquids plotted on this diagram are plagioclase-saturated and outline the olivine-augite (*aug*)-plagioclase, olivine-pigeonite (*pig*)-plagioclase and olivine-orthopyroxene (*opx*)-plagioclase saturation surfaces. *Crosses* are experiments of Walker et al. (1979) on Oceanographer Fracture Zone (*OFZ*) basalts. Symbols for Medicine Lake Highland experiments are: *diamonds* = Modoc HAB, *squares* = OPOA, *triangles* = Modoc BA, *circles* = LPOA. Microprobe analyses of liquids used for the projection are found in Table 2. This projection scheme is calculated by converting wt.% oxides into mole %. Alkalis and alumina are converted to $NaO_{0.5}$, $KO_{0.5}$ and $AlO_{1.5}$. Mineral components are calculated in the following manner:

$$\text{Sum} = SiO_2 - CaO - 2(KO_{0.5} + NaO_{0.5}) + Cr_2O_3 + TiO_2$$

$$\text{Qtz} = (SiO_2 - 0.5\,(FeO + MgO) - 1.5\,CaO - 0.25\,AlO_{1.5} - 2.75\,(NaO_{0.5} + KO_{0.5}) + Cr_2O_3 + 0.5\,TiO_2)/\text{sum}$$

$$\text{Plag} = 1/2(AlO_{1.5} + NaO_{0.5} - KO_{0.5})/\text{sum}$$

$$\text{Oliv} = 1/2\,(FeO + MgO + 1/2\,(AlO_{1.5} - KO_{0.5} - NaO_{0.5}) - CaO - 2\,TiO_2 - Cr_2O_3)/\text{sum}$$

$$\text{Cpx} = CaO - 1/2\,AlO_{1.5} + 1/2\,(KO_{0.5} + NaO_{0.5})/\text{sum}$$

$$\text{Or} = KO_{0.5}/\text{sum}$$

$$\text{Sp} = (Cr_2O_3 + TiO_2)/\text{sum}$$

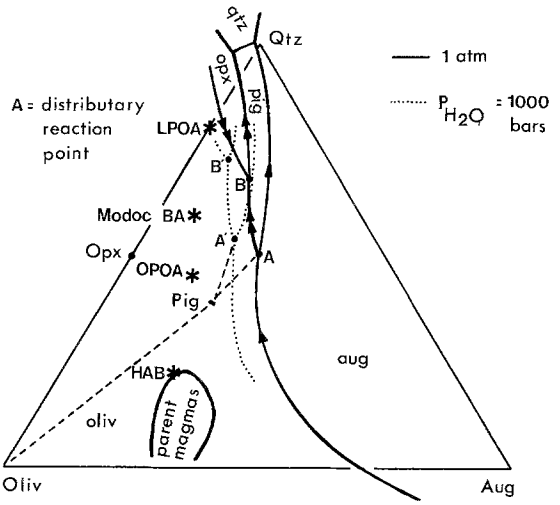

Fig. 4. Cotectics and reaction curves at 1 atmosphere and inferred at $pH_2O = 1{,}000$ bars. Pig and Opx mark the compositions of pigeonite ($Wo_{10\text{-}11}$) and orthopyroxene (Wo_2). Asterisks are the projected bulk compositions of the HAB, OPOA, Modoc BA and LPOA lavas used for the experiments

49 wt.%, $FeO + Fe_2O_3$ of 8 to 11 wt.% and low K_2O (0.10 to 0.20 wt.%). The isotopic and trace element characteristics have varied considerably through time, and will be discussed in a later section. The mixing of HAB and rhyolite documented at Chimney Crater and Glass Mountain links the basalt and silicic lavas, and our petrogenetic model necessarily begins with fractionation processes that operate on the HAB parent.

Low Pressure Phase Relations

Since the crystallization histories of the Medicine Lake Highland lavas involve plagioclase, olivine, augite, pigeonite and orthopyroxene, a projection scheme based on these components is used to display compositional variation. O'Hara's (1968) CMAS projection has been modified for this purpose. The microprobe analyses of experimentally produced liquids are recalculated from wt.% oxides to mole % of the components olivine, plagioclase, orthoclase, clinopyroxene, silica and spinel, and 6-component space is simplified by projection into the tetrahedron olivine-clinopyroxene-plagioclase-silica. The subprojection from plagioclase to olivine-clinopyroxene-silica (Fig. 3) is similar to that used by Walker et al. (1979), differing in the exclusion of orthoclase from the plagioclase component and in calculation of chromite + ulvöspinel as an additional component. Glasses coexisting with plagioclase, olivine and pyroxene are used to construct the cotectics, reaction curves and reaction points in Fig. 3. This projected phase diagram, though similar to the system forsterite-diopside-silica of Kushiro (1972b) and Longhi and Boudreau (1980) differs in several respects. The major difference is that the 5-phase point olivine-augite-pigeonite-plagioclase-liquid is a distributary reaction point (pt. A, Fig. 4). In the system forsterite-diopside-silica point A is a reaction point. The protoenstatite field is also absent in this iron and alkali-bearing system.

The projection scheme is useful for calc-alkaline series rocks, but may not be strictly applicable for low-alkali silica-rich suites. K_2O contents vary from 0.12 wt.% to ~1.5 wt.% in the andesites and to ~4 wt.% in the rhyolites. The $Fe^{2+}/(Fe^{2+} + Mg)$ also increases from mafic to silicic members, and different iron enrichment trends may have slightly different cotectic topologies (Longhi and Boudreau 1979). There are 3 reaction curves in the pseudoternary: olivine + pigeonite + plagioclase, olivine + orthopyroxene + plagioclase and orthopyroxene + pigeonite + plagioclase. At the olivine-pigeonite-orthopyroxene-plagioclase-liquid point (pt. B, Fig. 4) olivine + liquid react to orthopyroxene + pigeonite.

Crystallization, Assimilation and Mixing Paths

Under the conditions of the experiments equilibrium crystallization for Modoc HAB involves olivine + plagioclase separation until the liquid intercepts the olivine-plagioclase-augite cotectic. The 3-phase assemblage crystallizes and the liquid follows the cotectic to the distributary reaction point A (Fig. 4). Here augite, olivine and liquid react to pigeonite, the liquid becomes iron-enriched at a constant silica value and is exhausted. Compositions that lie within the triangle Oliv-Aug-Pig in Fig. 4 will crystallize completely at point A. Under conditions of fractional crystallization an HAB liquid will crystallize olivine + plagioclase, become augite saturated and follow the augite-olivine-plagioclase cotectic to point A. Since point A is a distributary reaction

point, there exist two possible fractionation paths. One path follows the olivine-pigeonite-plagioclase reaction curve and the other follows the augite-pigeonite-plagioclase cotectic. In the case of perfect fractionation only the augite-pigeonite-plagioclase curve may be followed, because both olivine and augite are removed from reaction with the liquid. Olivine must be present in reaction with liquid for the olivine-pigeonite-plagioclase reaction curve to be followed. In general, bulk compositions that lie in the region defined by Oliv-Pig-A-Aug (Fig. 4) follow the pigeonite-augite-plagioclase cotectic during fractional crystallization to the pigeonite-augite-plagioclase-quartz eutectic.

Fractional crystallization paths for compositions that plot above the lines Oliv-Pig-A move away from olivine to the olivine-pigeonite-plagioclase reaction curve. Olivine is removed from reaction and the liquid moves into the pigeonite + plagioclase primary phase volume away from pigeonite and intercepts the pigeonite-augite-plagioclase cotectic. Crystallization of pigeonite, augite and plagioclase drives the liquid to the pigeonite-augite-plagioclase-quartz eutectic.

Bulk compositions that lie above the line Oliv-B in Fig. 4 will follow fractionation paths away from olivine to the olivine-orthopyroxene-plagioclase reaction curve. Olivine is removed from reaction and the liquid's composition moves into the orthopyroxene + plagioclase primary phase volume, following a path away from orthopyroxene. The liquid reaches the reaction curve orthopyroxene-pigeonite-plagioclase, orthopyroxene is removed from reaction and the liquid follows a path away from pigeonite through the pigeonite + plagioclase primary phase volume to the augite-pigeonite-plagioclase cotectic or the pigeonite-quartz-plagioclase cotectic, depending on the bulk composition. Finally, the liquid reaches the pigeonite-augite-plagioclase-quartz eutectic.

The presence of the distributary reaction point A precludes any low-pressure fractional crystallization relation between an HAB parent and the compositionally evolved OPOA, Modoc BA and LPOA (Fig. 4). The phase appearance sequence observed in these samples and in the HAB (Fig. 2) is as predicted in the preceeding discussion. The OPOA, Modoc BA and LPOA reach olivine-pigeonite-plagioclase or olivine-orthopyroxene-plagioclase reaction curves. During fractional crystallization an HAB will not follow these cotectics. Instead, the liquid line of descent departs from point A and follows the augite-pigeonite-plagioclase cotectic.

Three processes can allow an HAB parent to approach the compositions above the Oliv-Pig-A line and thereby fractionate along the pigeonite and orthopyroxene-saturated liquid lines of descent. The first process is fractionation at elevated water pressures. Eggler (1972) investigated the crystallization of a Paricutin andesite under conditions of elevated pressure and variable pH_2O. An increase in pH_2O suppresses the plagioclase stability field, expands the clinopyroxene field and causes the orthopyroxene field to encroach on the olivine primary phase volume. Eggler's experiments on Paricutin lava FP-16-52 located a multiple saturation point olivine-plagioclase-orthopyroxene-pigeonite(?)-liquid at $pH_2O = 1{,}000$ bars, and the position of this reaction point (B′) is obtained by projecting the composition of FP-16-52 into the pseudoternary (Fig. 4). Point B′ and, by inference, point A′ are at higher SiO_2 values than their low pressure equivalents and the accompanying cotectic shifts shrink the olivine field and expand the orthopyroxene and augite fields.

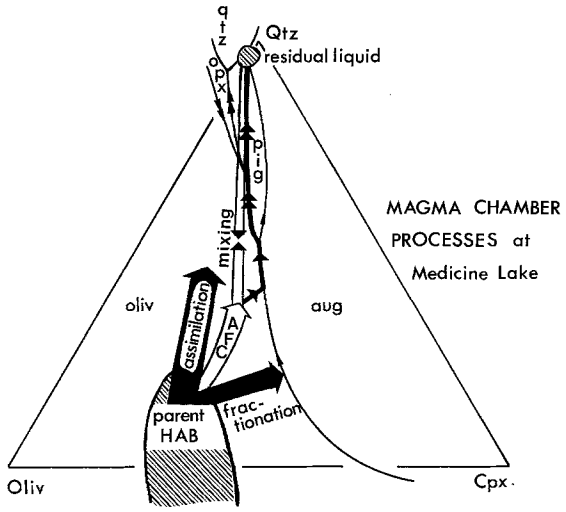

Fig. 5. A summary of the magma chamber processes that operated to form Medicine Lake lavas. Parental HAB undergoes both fractional crystallization and assimilates a crustal component which alters its composition. Subsequent fractional crystallization of HAB produces dacite and rhyolite residual liquids. The assimilation vector projects toward rhyolite, a likely first liquid composition produced by partially melting wallrock and xenoliths. Mixing of rhyolite and HAB generates Modoc BA, LPOA and dacite lavas

The shift in cotectics caused by increased pH_2O allows parental HAB to fractionate to liquids similar to the OPOA and the Modoc BA. Fractional crystallization of HAB at elevated H_2O pressure begins with a smaller interval of olivine (± plagioclase) removal. The high pressure olivine-augite-plagioclase cotectic is reached and cotectic crystallization moves liquids over the 1 atmosphere Oliv-Pig-A barrier toward the distributary point A′ (Fig. 4). If cotectic liquids that lie above Pig-A are separated from their crystal residues and moved to shallow-level magma reservoirs or erupted to the surface, lavas with the characteristics of OPOA and Modoc BA are produced. Point A′ remains a distributary reaction point and liquids that lie below the line Oliv-Pig-A′ will follow the pigeonite-augite-plagioclase cotectic as fractionation advances at $pH_2O = 1{,}000$ bars. Thus, A′ prevents the production of andesite liquids (LPOA in Fig. 4) by fractionation of HAB at $pH_2O = 1{,}000$ bars.

A second process, assimilation, assists fractionation in moving liquids to compositions above the line Oliv-Pig-A. A parent HAB magma injected into continental crust heats and partially melts its surroundings subject to the limitations pointed out by Bowen (1928, chap. 10). The first melt produced from an assumed graywacke or argillite contaminant is rhyolitic; higher percentages of partial melting could produce dacite. Thus, an assimilation vector (Fig. 5) drives liquids toward the silica-rich eutectic. Crystallization of HAB must accompany assimilation to provide the heat necessary to melt the surrounding rock and the resultant is combined assimilation and fractional crystallization or AFC (O'Hara 1977; Taylor 1980; DePaolo 1981). The AFC vector illustrated in Fig. 5 shows a possible trajectory for olivine fractionation + assimilation. At reaction point A or A′, AFC moves the bulk composition into the pigeonite + plagioclase primary phase volume, assuming rhyolite as the assimilant. If dacite is the assimilant, AFC allows liquids

to follow the olivine + pigeonite + plagioclase reaction curve.

The third process, magma mixing, generates lavas of intermediate composition by mixing an HAB parent with a rhyolite produced through the processes of fractionation or AFC. Fractional crystallization of HAB through point A or A′ and down the pigeonite-augite-plagioclase cotectic to the eutectic oliv-aug-pig-qtz will produce rhyolite residual liquids. Mixing of a fresh parental HAB magma and the rhyolite creates intermediate compositions that lie above the oliv-pig-A line. A similar mixing process could involve rhyolite melts generated by fractionation + assimilation.

Compositional Variations Among Medicine Lake Lavas

Major Elements

In the previous section we demonstrated that the Medicine Lake lavas chosen for the experiments could not be related through low pressure fractional crystallization of an HAB parent, and we discussed three processes which allowed a parental HAB to yield liquids similar to OPOA, Modoc BA and LPOA. In this section we discuss major element compositional variations observed in analyzed samples from Medicine Lake Highland using the data of Barsky (1975), Condie and Hayslip (1979) and Mertzman (1977a, b, 1979). The results of our experiments and those of Eggler are used to test the possibility that the observed compositional spread was produced by fractionation, involving olivine + plagioclase + clinopyroxene, amphibole or magnetite at high f_{O_2}. We conclude that oliv + plag + cpx fractionation + assimilation + mixing combined to produce the observed compositional variations.

Analyses of Medicine Lake volcanics are assumed to represent liquid compositions and are plotted in the pseudoternary planes olivine-diopside-silica (Fig. 6) and olivine-plagioclase-quartz (Fig. 7). $FeO + Fe_2O_3$ was calculated using the Sack et al. (1980) estimation technique and the resultant FeO was used in the projection calculation. The QFM buffer and temperatures of 1,200° C for HAB, 1,100° C for andesite and 1,000° C for dacite and rhyolite were assumed. The compositional trend in Fig. 6 shows a linear variation from Modoc HAB to rhyolite and dacite. In other subprojections (Fig. 7) and in oxide-oxide variation diagrams (Fig. 8) a single linear trend is not visible. If it is assumed that magma mixing produced the trends, the olivine-plagioclase-silica diagram shows several mixed lava groups. Mixing lines originating at rhyolite, and drawn through each group (Modoc BA, OPOA and PA) project to a variety of HAB parents (Fig. 7b). The projections and the oxide-oxide plots show permissive evidence for mixing, but the trends are not obvious. The composition of phenocryst assemblages and textural criteria provide supportive evidence (Gerlach and Grove 1982), and some lavas (Glass Mountain dacite, Modoc BA, LPOA) can be identified as mixtures of Mg-rich parental HAB and rhyolite. Other volcanic units (Lake Basalt, OPOA, PA) show evidence of mixing a compositionally evolved basalt parent and rhyolite, whereas others lack evidence for magma mixing.

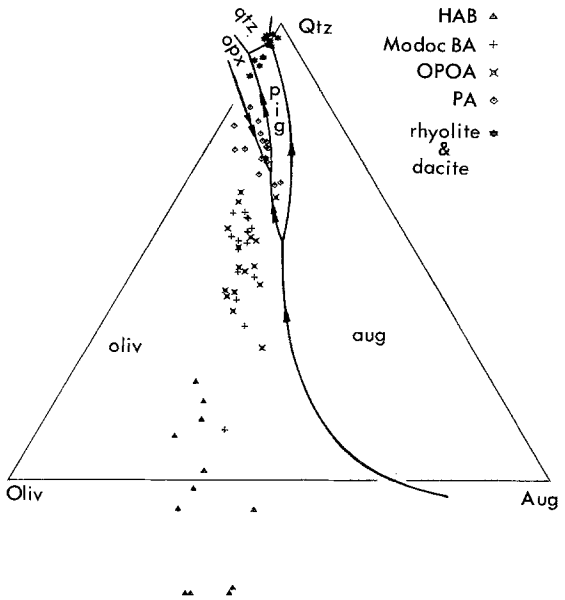

Fig. 6. Compositions of Medicine Lake Highland volcanics projected into the pseudoternary olivine-clinopyroxene-silica. Cotectics are taken from Fig. 3

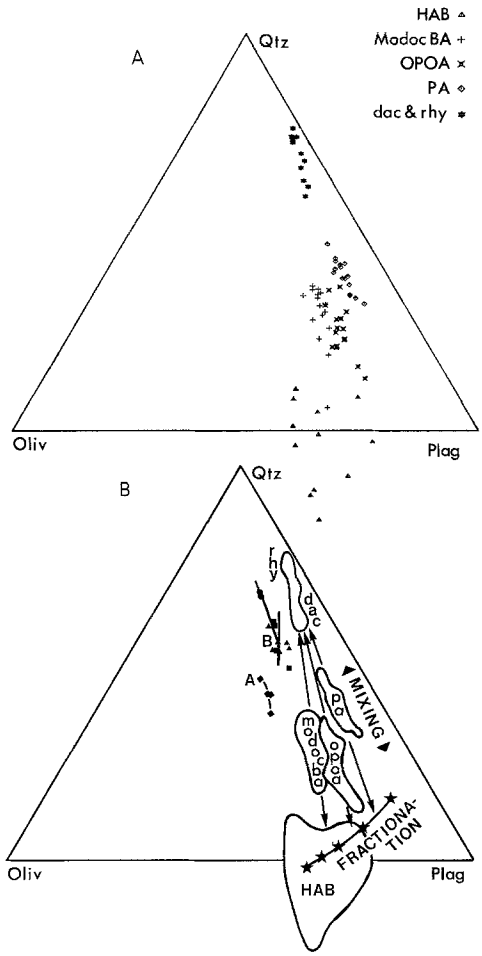

Fig. 7. A Compositions of the volcanics at Medicine Lake projected on the pseudoternary olivine-plagioclase-silica. **B** The fields for the lavas plotted in (A) are outlined. Also shown are the projected compositions of the multiply saturated experiments and points *A* and *B* (symbols are defined in Fig. 3). *Stars* show the projected compositions of the fractionation calculation (Table 6). The *arrows* illustrate how mixing between an HAB of variable composition and rhyolite produces the Modoc BA, OPOA and PA lavas

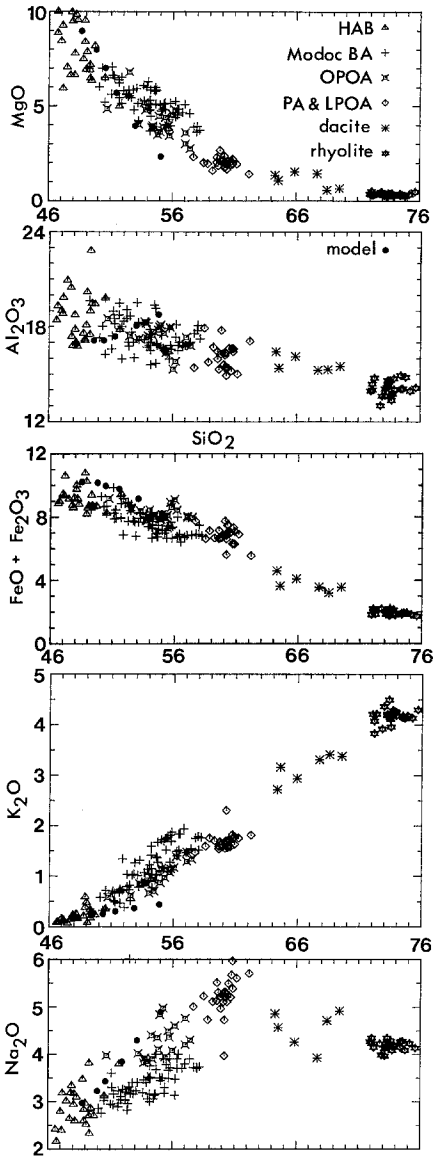

Fig. 8. Harker variation diagrams show the compositional variations among Medicine Lake lavas. Solid dots are the fractionation calculation (Table 6) plotted in 0.1 increments of F (% of liquid remaining) from F = 1.0 to F = 0.5

Fractionation Models for Major Element Variation

Olivine + Plagioclase + Clinopyroxene Fractionation. Several OPOA lavas studied by Gerlach and Grove (1982) do not contain textural or petrographic evidence for mixing of an Mg-rich basalt with rhyolite prior to eruption. We assumed that fractional crystallization of HAB at elevated pressures produced these lavas, and calculated a fractional crystallization path that approached the composition of these OPOAs. Warner basalt was chosen as the parent (Table 6) and removal of olivine + plagioclase in weight proportions (50:50) followed by olivine + clinopyroxene + plagioclase in the weight proportions (30:30:40) reproduced the compositions of silica-poor OPOAs after 50% fractionation. This assumed fractionation path could occur at moderate crustal pressures (1 to 3 kbar) and water-undersaturated conditions. The calculated fractionation path (Fig. 7b and Fig. 8) approaches the compositions of the OPOAs on the projection scheme and on the variation diagrams for MgO, FeO + Fe_2O_3 vs. SiO_2, but departs for Al_2O_3 and K_2O vs. SiO_2. The lack of agreement between calculated K_2O abundance and that observed in the OPOAs is extreme, and the intermediate lavas are 2 to 3 times higher in K_2O than calculated by the fractionation model.

Fractionation Models for Major Element Variation

Amphibole Fractionation. The effects of amphibole fractionation on major and trace element abundances are poorly understood, and distribution coefficients vary widely depending on the composition of the melt and amphibole (Cawthorn 1976; Irving 1978). Amphibole fractionation would require high pressures and high water contents ($P >$ 8 kbar and 3 wt.% H_2O, Eggler and Burnham 1973). Geophysical evidence permits the existence of a shallow magma chamber beneath Medicine Lake Highland (Finn and Williams 1982). Though the presence of shallow magma reservoirs does not preclude the possibility that amphibole fractionation played a role at Medicine Lake Highland, we find no petrographic evidence for amphibole early in the petrogenetic history. Amphibole occurs only rarely at Medicine Lake in the dacite and rhyolite glass flows (Mertzman and Williams 1981). The amphibole reported by Mertzman (1978) from Little Mount Hoffman HAB is compositionally similar to those found in the silicic magmas, and was probably incorporated during magma mixing. Thus, we reject amphibole fractionation because we cannot model the process and because we see no petrographic evidence for early amphibole crystallization.

Fractionation Models for Major Element Variation

Magnetite Fractionation. Osborn (1959) discussed the effects produced by fractional crystallization under variable f_{O_2} conditions, and suggested that the iron-enrichment (tholeiitic) and the iron-depletion (calc-alkalic) trends could be produced by crystallizing the same parental magma at different oxygen activities. Osborn proposed that the tholeiitic trend formed under conditions of low f_{O_2} crystallization. The phase diagram (Fig. 4) confirms this prediction; parental basalt magma crystallizes to the distributary reaction point A or A′ and undergoes iron enrichment at constant silica contents until olivine and augite are removed from contact with the liquid. Osborn proposed that magnetite crystallized as a liquidus phase under oxidizing conditions and allowed the early silica enrichment and iron depletion characteristic of the calc-alkalic series. Osborn's hypothesis was tested experimentally using the Modoc intersertal HAB parent. Fractional crystallization experiments were performed at linear cooling rates at an f_{O_2} of the NNO and QFM buffer, and isothermal experiments were performed 2 and 4 orders of magnitude above the QFM buffer. The iron-enrichment trend is followed in the low pressure cooling rate experiments, as shown when the liquid compositions from these experiments are compared with the Medicine Lake lavas on FeO*/MgO vs. SiO_2 and FeO* plots (Fig. 9, FeO* = FeO + 0.9 Fe_2O_3). The contrasting trends parallel the tholeiitic and calc-alkalic trends as defined by Miyashiro (1974). Experimentally produced iron-enrichment occurs at the distributary point, where the reaction of olivine + augite ↔ pigeonite occurs at constant silica values. When olivine and augite are removed from reaction, augite + pigeonite + plagioclase crystallization changes the

Table 6. Fractionation and combined assimilation-fractionation models

Wt% oxides	Starting compositions[a]			Fractional crystallization[b]					Assimilation + Fractional crystallization[c]										OPOA with[d] 55% SiO_2		Calculated residual[e] liquids with 55 wt.% SiO_2		
	Parent	Assimilant		0.90	0.80	0.70	0.60	0.50	0.90		0.80		0.70		0.60		0.50						
		R	G						R	G	R	G	R	G	R	G	R	G			FC	AFC R	AFC G
SiO_2	48.50	73.10	68.00	49.80	50.50	51.40	53.00	55.00	49.90	49.90	51.20	51.10	52.50	52.40	54.00	53.80	56.30	55.90	54.91	55.24	55.00	55.20	55.00
Al_2O_3	17.00	14.00	14.50	17.20	17.20	17.50	18.00	18.70	17.10	17.10	17.10	17.10	17.10	17.10	17.10	17.20	17.20	17.30	17.98	17.58	18.70	17.10	17.30
FeO	10.00	1.80	3.00	9.96	9.83	9.68	9.08	7.80	9.89	9.90	9.70	9.75	9.53	9.60	9.18	9.29	8.34	8.52	7.85	7.99	7.80	8.80	8.60
TiO_2	0.60	0.20	0.25	0.67	0.74	0.87	1.07	1.31	0.66	0.66	0.75	0.75	0.85	0.85	0.96	0.97	1.14	1.15	1.11	1.23	1.31	1.05	1.12
MnO	0.17	0.01	0.11	0.19	0.21	0.25	0.30	0.37	0.18	0.19	0.21	0.21	0.24	0.24	0.27	0.28	0.32	0.33	0.15	0.16	0.37	0.29	0.32
MgO	9.00	0.40	1.50	7.98	7.00	5.75	4.03	2.32	8.01	8.03	6.77	6.81	5.69	5.76	4.60	4.68	3.14	3.25	4.45	3.87	2.32	3.86	3.43
CaO	10.50	1.50	2.20	10.80	10.70	10.30	9.75	9.12	10.70	10.70	10.30	10.40	9.74	9.79	9.11	9.18	8.22	8.32	7.99	7.51	9.12	8.66	8.43
Na_2O	3.00	3.85	3.80	3.23	3.44	3.80	4.32	4.88	3.22	3.22	3.50	3.49	3.80	3.80	4.10	4.10	4.48	4.48	4.10	4.97	4.88	4.30	4.44
K_2O	0.20	4.05	2.70	0.22	0.25	0.29	0.36	0.44	0.26	0.25	0.36	0.32	0.47	0.41	0.64	0.51	0.80	0.66	0.87	0.97	0.44	0.70	0.64
Rb (ppm)	1	160	60	1	1	1	2	2	3	2	6	3	9	4	13	6	19	8	20	20	2	16	8
Sr (ppm)	390	100	250	404	418	445	484	526	400	402	413	417	428	435	443	452	464	477	656	588	526	453	474
Ni (ppm)	200	3	0	56	19	6	1	0	66	66	20	20	7	7	3	3	1	1	17	2	0	1	1
$^{87}Sr/^{86}Sr$	0.7029		0.7095																				

[a] The parental high-alumina basalt used for the fractionation calculation is a combination of Warner basalt analyses from Mertzman (1977b). Two assimilant end-members were tested in the AFC model. The first (R) is an average of Glass Mountain rhyolites reported by Mertzman and Williams (1981). The second (G) is a graywacke with trace element characteristics chosen to be typical of those found in eugeosynclinal sediments from Oregon and California (Peterman et al. 1967). The major element composition was taken from Pettijohn (1975, Table 7–9)

[b] The fractional crystallization started with Warner basalt and removed variable proportions of olivine, plagioclase and clinopyroxene to approach the composition of the low SiO_2 members of the OPOA lavas. The calculation used weight units, and equilibrium phase compositions were removed at each fractionation increment using our experimentally determined Fe-Mg exchange partition coefficients for olivine and clinopyroxene ($K_D^{Fe\text{-}Mg} = X_{Fe}^{xtal} X_{Mg}^{liq} / X_{Mg}^{xtal} X_{Fe}^{liq}$, X = normalized atom fraction) of 0.29 and 0.25. The clinopyroxene in the calculation was $Ca_{0.44}$ $FeMg_{0.52}$ $Al_{0.04}$ $Si_{1.96}$ $Al_{0.04}$ O_6. Ni fractionation was calculated assuming a partition coefficient (K_d) of 20 for olivine (Hart and Davis 1978) and 5 for clinopyroxene (Irving 1978). The Ca-Na exchange partition coefficient for plagioclase ($K_D^{Ca\text{-}Na} = X_{Ca}^{xtal} X_{Na}^{liq} / X_{Na}^{xtal} X_{Ca}^{liq}$) was obtained from our experiments and was varied continuously during the calculation from 1.2 to 0.8. Sr fractionation was calculated assuming a K_d of 1.5 (Drake and Weill 1975). The calculation was carried out in increments of 5 wt.% solid removed from the residual liquid. Liquid composition was determined by multiplying the wt.% oxide in each phase × weight proportion of the phase × 0.05. The resultant liquids were normalized to 100%. Thus, the fraction of liquid remaining (F) changed at each increment as 0.95^n, where n = the number of increments. The calculation reported above assumed the removal of oliv: plag:cpx in the proportions (50:50:0) from F = 1.0 to 0.86 and (30:40:30) from F = 0.86 to F = 0.5. Liquid compositions are reported at fractionation increments of 0.1

[c] In these calculations an assimilant was added to the liquid and solids were removed through fractionation. The value of the ratio of the mass of assimilant added/mass of solids removed (r) was set at 0.11. This AFC calculation used the same phase proportions as the fractionation calculation. Liquid compositions are reported at fractionation increments of 0.1. The R liquid has assimilated a minimum melt component represented by rhyolite. The G liquid has assimilated graywacke

[d] Compositions of OPOAs (Metzman 1977b) that contain ~55 wt.% SiO_2 obtained by fractional crystallization (FC) and by combined fractional crystallization and assimilation of rhyolite (AFC R) and graywacke (AFC G)

[e] Compositions of residual liquids with 55 wt.% SiO_2 obtained by fractional crystallization (FC) and by combined fractional crystallization and assimilation of rhyolite (AFC R) and graywacke (AFC G)

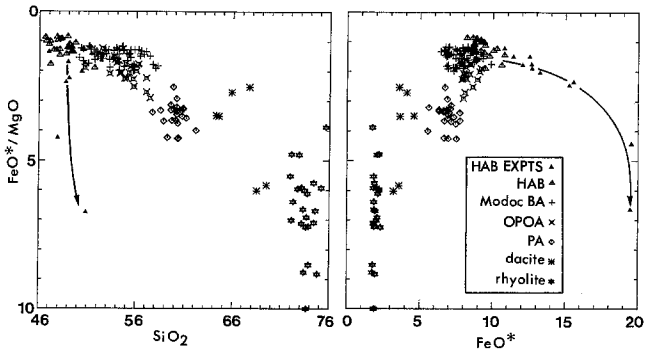

Fig. 9. FeO*/MgO plotted against SiO_2 and FeO* (FeO* = FeO + 0.9 Fe_2O_3). Miyashiro (1974) used these coordinates to discuss calc-alkalic vs. tholeiitic differentiation trends. The Medicine Lake lavas follow a calc-alkalic trend, while residual liquids produced by crystallization of HAB (Tables 2 and 4) outline the tholeiitic trend

liquid composition rapidly to the SiO_2-rich cotectic. Immiscible liquids of dacite and ferrobasalt form at the highest percentages of crystallization. (The compositions are not reported because the small size of the immiscible blebs prohibited quantitative analysis). Kuno (1965) found evidence for a similar fractionation path in Warner HAB lava flows.

The AFM projection also shows the characteristic iron-enrichment path followed by Modoc HAB (Fig. 10) when crystallized at the QFM and NNO buffer. The isothermal experiments performed at high f_{O_2} show early alkali enrichment and iron depletion, and as suggested by Osborn (1959), the early magnetite precipitation can produce a calc-alkalic trend. Fractional crystallization of the Modoc intersertal-porphyritic BA also follows a calc-alkalic trend (Fig. 10), which would be predicted by the phase diagram (Fig. 4). The Modoc BA lies above the line Oliv-Pig-A and fractionates along orthopyroxene and pigeonite-saturated curves to andesite, dacite and rhyolite residual liquids.

The Medicine Lake Highland lavas follow the AFM trend characteristic of the calc-alkalic series (Fig. 10a). Note that the loss of ~30% Na_2O displaces the experiments to lower $K_2O + Na_2O$ proportions (Fig. 10b). Despite the limitations imposed by alkali loss, the contrasting fractionation trends are recognizable. The Modoc HAB parent crystallized along a line of iron-enrichment, and because Modoc BA is compositionally evolved the calc-alkalic trend is followed during fractionation. The high f_{O_2} experiments begin a trend that may follow a calc-alkalic line, and crystallization under oxidizing conditions can not be ruled out, in general, as a means for generating an iron-depletion and silica-enrichment trend. However, there is no evidence for the required high f_{O_2} in the Medicine Lake lavas. Magnetite-ilmenite pairs from Medicine Lake dacites indicate f_{O_2} near QFM buffer (Gerlach and Grove 1982), and oxygen fugacity estimates from other Cascade volcanoes yield f_{O_2} near the NNO buffer (Drory and Ulmer 1974; Anderson 1975).

In addition, fractional crystallization at high f_{O_2} also fails to account for the large increases in K_2O (Fig. 8) from HAB (0.1 to 0.2) to OPOA lavas (0.6 to 1.0). Consequently, some of the major element variations in Medicine Lake lavas are consistent with fractional crystallization of olivine + plagioclase + clinopyroxene ± magnetite, but these fractionation models cannot reproduce the large increases in incompatible elements such as K_2O.

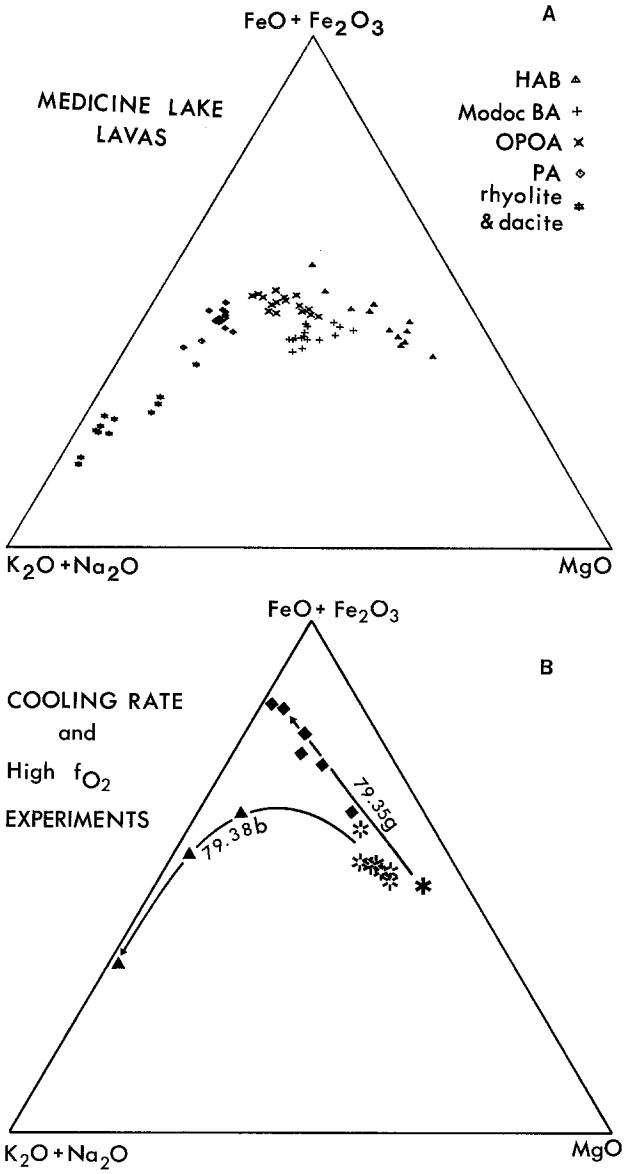

Fig. 10. **A** AFM diagram for Medicine Lake Highland volcanics. **B** Cooling rate and high f_{O_2} experiments are plotted on the AFM diagram. *Diamonds* are highly fractionated liquids produced in cooling rate experiments on the HAB at the QFM buffer. The *snowflake symbols* are experiments performed at 2 and 4 orders of magnitude above QFM. These high f_{O_2} experiments begin a calc-alkalic trend but have a higher Na/K ratio than the Medicine Lake lavas. The *triangles* are fractionated residual liquids from cooling rate experiments on 79-38b. These liquids follow the calc-alkalic trend

Trace Elements

Medicine Lake volcano has been the subject of several earlier geochemical studies incorporating trace-element and isotopic analyses (Barsky 1975, Condie and Hayslip 1975; Mertzman 1977a, b, 1979). In this section we focus on elements which are useful in identifying the relative roles of fractional crystallization, assimilation and mixing. For example, elements which are highly compatible with respect to the crystallizing assemblage are strongly controlled by fractionation, whereas elements which have low abundances in parental HAB relative to crustal rocks are sensitive to assimilation.

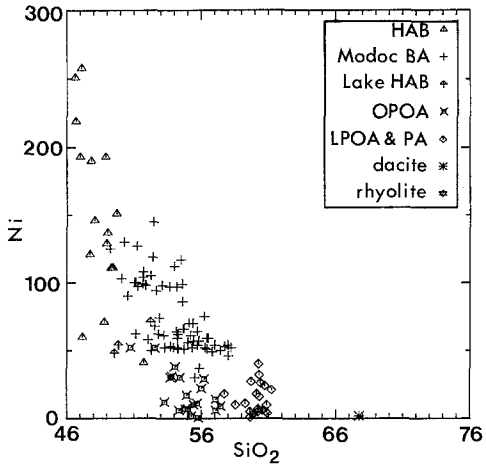

Fig. 11. Ni (ppm) vs. SiO_2 (wt.%) variations for Medicine Lake lavas

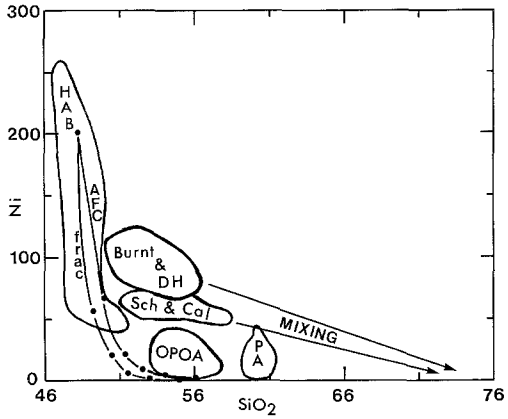

Fig. 12. Ni vs. SiO_2 variations from Fig. 11 showing the fields of eruptive units. Burnt and DH outline the Ni data from Burnt lava flow and Devil's Homestead flow while Sch and Cal outline the Ni values for the Schonchin and Callahan flows. The fractionation (*frac*) and AFC calculations from Table 6 are plotted as *solid dots*. Each *dot* is a 0.1 increment in F (F = % of liquid remaining) from F = 1.0 to F = 0.5. *Lines with arrows* show how mixing of rhyolite (assumed to be low in Ni) and HAB can produce the Ni variations observed in the Modoc BAs

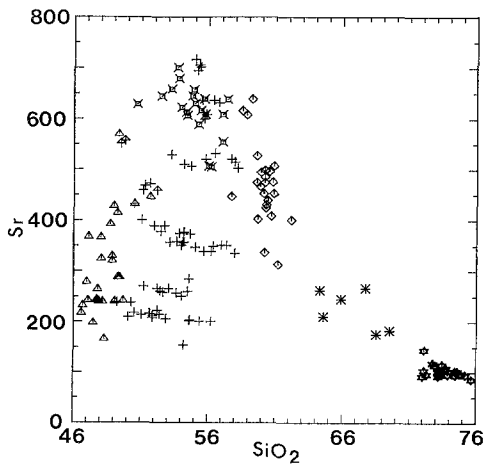

Fig. 13. Sr (ppm) vs. SiO_2 (wt.%) for Medicine Lake lavas. Symbols are described on Fig. 11

Unfortunately the trace element data set available from the literature is of limited use because of incomplete data for some elements and poor documentation of sample locations in some cases. Because most samples analyzed for trace elements were not identified in terms of Anderson's stratigraphy for the volcano, we have arbitrarily reclassified those samples which could not be assigned on the basis of location using compositional criteria (e.g. HABs have less than 3 ppm Rb and less than 51% SiO_2). Despite these difficulties, the trace-element data provide some important petrogenetic constraints.

Compatible Elements: Ni and Sr

Variations in abundances of trace elements which are compatible with respect to minerals in the low-pressure crystallization assemblage are consistent with an important role for fractionation in the petrogenesis of Medicine Lake lavas. Figure 11 displays the behavior of Ni, which is strongly partitioned into olivine and clinopyroxene. The steep drop in Ni concentrations in the HAB can be explained by the efficient extraction of this element from the melt by olivine and augite. The OPOA and PA groups have similar Ni contents ranging from less than 5 ppm to slightly over 50 ppm. The Ni abundances in Modoc BAs are higher than those of the OPOAs and PAs. Such elevated Ni concentrations are not consistent with fractionation; the calculation reported in Table 6 predicts 20 to 1 ppm Ni in lavas with the major element compositions of Modoc BAs. As shown in Fig. 12 the Modoc BAs form elongate fields which represent individual flows. The direction of elongation can be produced by mixing basalt with rhyolite (no analyses of Ni in rhyolite are reported, but Ni abundance is low, if similar to other calc-alkaline rhyolites). The highest Ni contents at 60% SiO_2 (20 ppm) are found in LPOA lavas, which show textural and phase chemistry evidence for mixing of basalt and rhyolite. Other OPOA and PA lavas require mixing of Ni-rich and Ni-poor mafic magma with rhyolite.

Plagioclase has played an important role in the petrogenesis of these rocks, as evidenced by petrographic observations and the results of our crystallization experiments. Variations in the Sr contents of HAB parent magmas, changes in the proportion of phases in the crystallizing assemblage and variations caused by the compositional dependence of D^{Sr}_{plag} combine to produce complicated Sr behavior (Fig. 13).

HAB's range widely in their Sr contents, from 150 to almost 600 ppm. OPOA lavas are characterized by uniformly high concentrations (600–700 ppm), most PAs are lower (400–550), and rhyolite values cluster around 100 ppm. Extreme diversity is found in the Modoc BA group, whose Sr contents span nearly the entire range found in all other rock types. Some individual flow units define elongate arrays that trend toward the rhyolite composition. As indicated schematically (Fig. 14), this elongation is consistent with late-stage mixing of rhyolite with more mafic Modoc magma. Sr concentrations in dacites can also be explained by mixing of rhyolite and less evolved compositions.

Lithophile Elements: Rb

In the Medicine Lake lavas Rb contents are positively correlated with SiO_2 (Fig. 15). Progressively higher Rb concen-

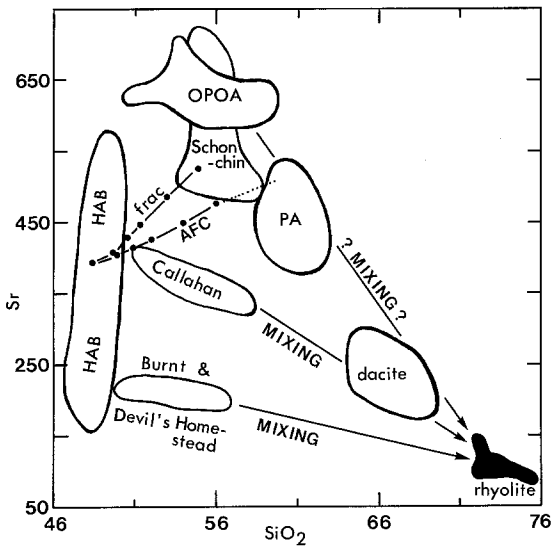

Fig. 14. Sr vs. SiO_2 variations from Fig. 13 with the fields of eruptive units outlined. HAB lavas show a wide variation in Sr content. Individual Modoc BA flows can be recognized on this plot as mixtures of low-Sr, high-SiO_2 rhyolite and HAB of variable Sr content. Mixing lines emphasize the expected Sr variations. The fractionation (*frac*) and AFC calculations from Table 6 are plotted as *solid dots*. Each *dot* represents a 0.1 increment in F (% of liquid remaining) from 1.0 to 0.5. The *dotted line* extending from the AFC calculation illustrates how continued AFC would produce some PA lavas

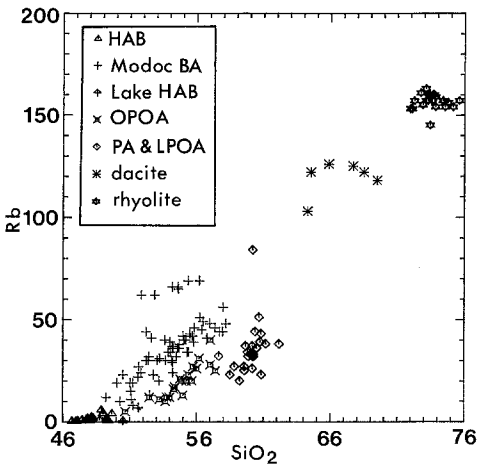

Fig. 15. Rb (ppm) vs. SiO_2 (wt.%) variations for Medicine Lake lavas

trations are found in the sequence HAB-OPOA-PA, and Rb variation in each lava type defines arrays which are elongated toward the rhyolite composition (Fig. 16). Dacites and rhyolites are distinct from other rock types, with Rb concentrations of 150–170 and 100–130 ppm respectively. All intermediate lavas have Rb concentrations in excess of those which can be produced by simple fractional crystallization of reasonable amounts of low pressure mineral assemblages from Medicine Lake HAB composition (Table 6). This statement applies to some other incompatible elements as well, and is characteristic of other calc-alkalic suites (Gill 1981). Both assimilation of Rb-rich crustal rock and mixing with more Rb-rich magma such as rhyolite are capable of producing such enrichments

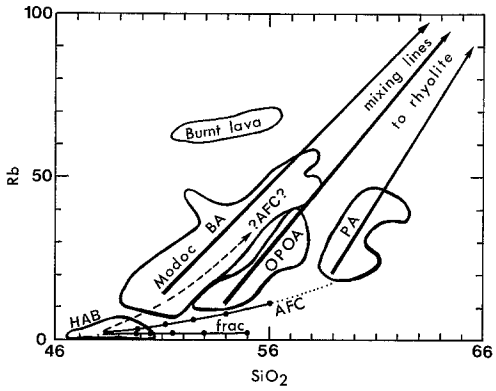

Fig. 16. Schematic Rb vs. SiO_2 relations similar to those for Ni (Fig. 12) and Sr (Fig. 14). Mixing lines, AFC and frac curves are the same as those described in Fig. 14. The *dashed AFC line* that enters the Modoc BA field schematically shows that a higher r value is required to produce the incompatible element (and isotopic) characteristics of Modoc BAs

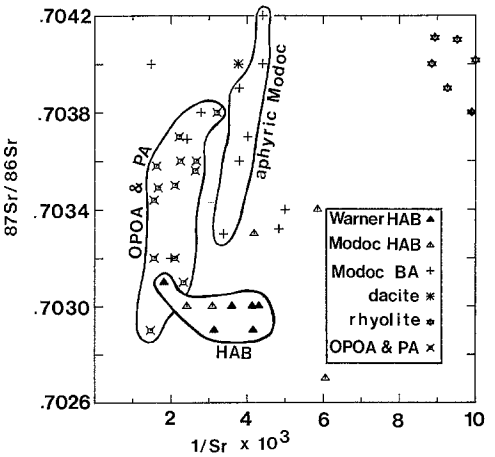

Fig. 17. $^{87}Sr/^{86}Sr$ vs. 1/Sr for Medicine Lake rocks. The figure shows existing and new analyses (Table 5). The aphyric Modoc BAs are those discussed by Mertzman (1979). The HAB field does not enclose the late highly variable Modoc HABs which range from 0.7027 to 0.7034

(Fig. 16), but discrimination between these two alternatives is difficult. This task requires integration of isotopic, textural and bulk chemical data, and is discussed in the next section.

Sr Isotopic Systematics

Figure 17 is a 1/Sr vs. $^{87}Sr/^{86}Sr$ diagram on which all available analyses of rocks from Medicine Lake are plotted (Mertzman 1979; Barsky 1975; Peterman et al. 1970) including data for nine of our samples (Table 5). The lavas form 4 broad groups: (1) Most HAB analyses fall in a field with roughly constant $^{87}Sr/^{86}Sr$ and Sr concentrations which vary from 230 to 620 ppm, although a few Modoc HAB samples vary more widely in $^{87}Sr/^{86}Sr$. (2) OPOA lavas are characterized by high Sr concentrations (430–670 ppm) which are negatively correlated with $^{87}Sr/^{86}Sr$ from 0.7029 to 0.7038. (3) Modoc BAs scatter widely in the region between the HAB and rhyolite fields. An aphyric subset of these analyzed by Mertzman also shows

a correlation between 1/Sr and 87/86. Rhyolites and dacites plot in a restricted range of $^{87}Sr/^{86}Sr$ (0.7039–0.7043), with Sr contents of around 100 and 225 ppm respectively. Thus, the lavas at Medicine Lake are quite heterogeneous with respect to isotopic composition, but there are some systematic aspects of their heterogeneity.

Some of the isotopic variability is inherited from the source regions of the Medicine Lake HABs, because HABs with <2 ppm Rb range in $^{87}Sr/^{86}Sr$ from 0.7027 to 0.7034. Consequently, at least this range is expected in lavas derived from the HAB. However, most andesites, dacites and rhyolites have higher $^{87}Sr/^{86}Sr$, and an additional process is required. Mertzman (1979) ascribed all the isotopic heterogeneity in HAB, OPOA and PA samples he analyzed to the source region, arguing that the correlation of Rb/Sr with $^{87}Sr/^{86}Sr$ was a mantle isochron (Brooks et al. 1976). Such correlations or pseudo-isochrons have been reported from other andesitic volcanoes in both continental and island-arc settings (Ewart et al. 1973; Klerkx et al. 1977). Interpretation of these arrays as mantle isochrons with age significance is based on the assumption that the measured Rb/Sr ratios of the lavas reflect those of the source region. Such an assumption seems unwarranted for these rocks, since many of their features suggest later modification by fractionation and magma mixing, both of which would change their Rb/Sr ratios. One important point favoring the mantle isochron model was the excellent linearity of Mertzman's data. However, when these data are plotted together with other published analyses and our analyses of aphyric OPOAs (Table 5), a much greater amount of scatter is observed.

The isotopic data can be explained if Medicine Lake lavas formed by the interplay of assimilation, fractional crystallization and magma mixing. Though isotopic heterogeneities exist in the parent basalt, the bulk of HAB data indicate that a relatively uniform magma composition with $^{87}Sr/^{86}Sr = 0.7029 - 0.7030$, <2 ppm Rb and 250–350 ppm Sr was supplied to the volcano throughout its history. The elongate field of HABs (Fig. 17) is consistent in slope with fractionation of the low pressure assemblage used in the AFC calculation, combined with assimilation of a small amount of wall rock such as the assumed graywacke composition (Table 6, $^{87}Sr/^{86}Sr = 0.7095$). However, the lavas are enriched in Sr, when compared to the AFC calculation reported in Table 6. De Paolo (1981) has discussed a model for generating the high Sr concentrations observed in the mafic lavas from many subduction zone volcanic complexes which invokes high proportions of assimilation to fractionation (r) and suppression of plagioclase fractionation by either increasing water pressure or suspending the neutrally buoyant crystals. We have attempted to apply his model to Medicine Lake rocks and found it impossible to generate the observed major element variations without involving substantial amounts of plagioclase (Table 6). Also, high ratios of r would produce a much steeper negative slope than is observed in the HAB array (Fig. 17), since incorporation of radiogenic Sr from the wall rock rapidly increases the $^{87}Sr/^{86}Sr$ of the magma. The high $^{87}Sr/^{86}Sr$ (0.7095, Table 6) assumed for assimilant, however, seems necessary to account for the strong elevation of $^{87}Sr/^{86}Sr$ in the Modoc BAs. A possible explanation for the discrepancy between the HAB trend and the model is that the evolution of HAB compositions may not take place in a shallow-level chamber; they could for example have been modified during ascent through the lower crust, or even pooled at the base of the crust, as suggested by Gill (1981, his Fig. 3.8). In that case, HABs may have interacted with country rocks of much different composition from our proposed graywacke assimilant; a high-Sr, low $^{87}Sr/^{86}Sr$ assimilant such as mafic igneous rock would be suitable for the observed HAB array. In summary, our AFC model (Table 6) fails to reproduce the high Sr contents of the intermediate rocks, which could result from errors in the assumed D_{Sr}^{plag} or in the inferred phase assemblage.

The strongest evidence of assimilation of high $^{87}Sr/^{86}Sr$ material is found in the OPOA and PA lavas which form an array with positive slope on Fig. 17 and are similar in this respect to lavas from other calc-alkaline volcanoes (James et al. 1976; Briqueu and Lancelot 1979). Briqueu and Lancelot (1979) and DePaolo (1981) have discussed the possible role of AFC in producing such trends. The decreasing Sr concentrations in the increasingly contaminated OPOA and PA lavas indicate a higher bulk D for Sr during this stage of magmatic evolution than during the HAB stage of evolution. The elevated D_{Sr} may be caused by an increased proportion of plagioclase crystallization in the fractionating assemblage, or by higher D_{Sr}^{plag} at these lower temperatures. The aphyric Modoc BAs follow a similar trend of increasing $^{87}Sr/^{86}Sr$ with decreasing Sr, which can be accounted for by the AFC process. Modoc lavas have higher Sr isotopic ratios at equal values of SiO_2 than their OPOA counterparts, suggesting higher r values. Evidence for mixing between rhyolite and HAB magma, which is a first-order feature of these rocks on many other diagrams, is lacking in Fig. 17, in large part because of the paucity of multiple samples from single flows. In any case, because of the compression of the diagram at high Sr contents, and the much higher Sr concentrations of Modoc BA's relative to rhyolite, effects of mixing would not be well-displayed. The large degree of scatter in Modoc analyses when all samples are plotted may be from several sources. First, the source regions for Modoc magmas are heterogeneous (all three HAB with $^{87}Sr/^{86}Sr \neq 0.7030 \pm 1$ are Modoc rocks). Secondly, many are more porphyritic than their OPOA counterparts; inhomogeneous distribution of phenocrysts would cause scatter on Fig. 17. This is suggested by the tighter array formed by aphyric rocks. Finally, mixing of up to 35% rhyolite into these magmas prior to eruption would shift their compositions a small but variable distance to the right on Fig. 17.

Rhyolites and dacites at Medicine Lake have the highest $^{87}Sr/^{86}Sr$ measured from the area, indicating the largest degree of interaction with crustal rocks, but we conclude that these magmas are not chemically equivalent to the assimilated component. Since dacites show abundant textural and chemical evidence of late stage mixing between rhyolite and more mafic magmas, their Sr isotope signature can be explained as a feature inherited from the rhyolite, which is the dominant component of the mix.

Origin of Medicine Lake Lavas by Fractionation, Assimilation and Magma Mixing

In the previous sections we considered the ways in which fractional crystallization, assimilation and magma mixing affect the liquid line of descent of an HAB parent magma. A fractional crystallization model using olivine + plagioclase + clinopyroxene approached the composition of

OPOA lavas, amphibole or magnetite crystallization were rejected as having played a major role in producing the compositional spectrum, and trace element and isotopic data indicated that assimilation and magma mixing accompanied fractionation in generating the Medicine Lake lavas. The variations in compatible element abundances (Ni and Sr) implied magma mixing and fractional crystallization. Lithophile element abundances (K and Rb) required that assimilation and magma mixing operated along with fractional crystallization. In the remainder of the paper we present a model for the compositional evolution of the Medicine Lake lavas, discuss the assimilation process and discuss experimental evidence of the density-composition relations that lead to magma mixing.

Compositional Evolution of Medicine Lake Lavas

The compositions of the parent HAB liquids indicate separation from a source residue at depths of 45–60 km (Stolper 1980). HAB magma blobs rise and fail to interact with their surroundings during ascent until reaching upper crustal levels where density differences impede further ascent (Marsh and Kantha 1978). Trapped in crustal magma chambers, the HAB assimilates crustal material and undergoes fractional crystallization. Eruptions sample the evolving magma chamber(s), providing the observed compositional spectrum.

The fractional crystallization model (Table 6) was designed to reproduce the evolution of the parent HAB in an upper crustal magma chamber. Notable deviations from the model are caused by magma mixing. The linear trends formed by Modoc BAs on Na_2O, MgO and K_2O vs. SiO_2 (Fig. 8) and on Ni, Sr and Rb diagrams (Figs. 11, 13, 15) result from mixing rhyolite with mafic lava. Other departures from the calculated fractionation path require assimilation of a crustal component. In Table 6 the compositions of unmixed OPOAs with 55% SiO_2 are compared with fractionation and AFC calculations. Both graywacke and rhyolite were calculated as assimilants and r was chosen as 0.11. The assimilation models produce values of Al_2O_3, MgO, K_2O, CaO, etc. comparable to those observed in the OPOA lavas. The AFC models also enrich Rb (Fig. 16) to values that could not be achieved solely by fractionation, and elevate Ni contents at comparable SiO_2 contents (Fig. 12). Under the assumptions of the model (Table 6), both fractionation and AFC (Fig. 14) fail to produce the Sr enrichments found in the OPOA (600 ppm). The HAB starting composition (390 ppm Sr) is enriched to 525 ppm by fractionation, and 450 or 475 ppm by the AFC models. Models that successfully reproduce the major element chemistry can not generate the Sr contents, a failure that may be related to variability in the Sr content of the HAB parent. Variations in Sr (Fig. 14) result from a combination of processes. Variability in HAB Sr contents is partly a source region characteristic. AFC produces some enrichment in Sr, and the low-SiO_2 members of the PA lavas and Modoc mixed rocks may have been produced by AFC of an HAB parent with variable Sr ($\sim$200 ppm for Burnt and Devil's Homestead and $\sim$400 ppm for Callahan and PA lavas). Fractionation models have not been calculated beyond 56% SiO_2, but by increasing the percentage of plagioclase and removing orthopyroxene/pigeonite + magnetite, a drop in Sr and an increase in SiO_2 could lead to rhyolite. Alternatively, the processes that generate rhyolite could be different from those that produce compositional variation in the mafic lavas. Finally, mixing of HAB and rhyolite has produced hybrid intermediate lavas: the Modoc BAs, the dacite, and some OPOA and PA lavas. Thus, Sr heterogeneity in the HAB parents, AFC and magma mixing have conspired to produce the complex Sr variations.

The Rb abundances indicate assimilation of a crustal component and variation in r through the eruptive history. As illustrated in Fig. 16 the AFC model ($r=0.11$, solid line) can elevate Rb to values observed in the low SiO_2 OPOAs and PAs. The elongation of the OPOAs and PA trends is produced by mixing of the mafic AFC-generated lava with rhyolite. The Modoc BA trend appears to be produced by mixing HAB and rhyolite, but $^{87}Sr/^{86}Sr$, Sr abundance and major elements show that assimilation at higher r ($r=$ 0.4, dashed line on Fig. 16) is required to produce the characteristics of the Modoc rocks. Major and trace elements indicate mixing of up to $\sim$30% rhyolite with mafic lava to produce the Callahan and Schonchin flows, but the Sr contents ($\sim$350 and $\sim$650 ppm) and $^{87}Sr/^{86}Sr$ (as high as 0.7038 and 0.7040) require the isotopic characteristics of these mixed lavas to be dominated by the AFC-produced basaltic end member. Mixing of rhyolite with 100 ppm Sr and $^{87}Sr/^{86}Sr$ of 0.7040 will not elevate $^{87}Sr/^{86}Sr$ sufficiently to the observed values. An elevated $^{87}Sr/^{86}Sr$ can be generated in the mafic member of the mix by performing AFC at high r on an HAB parent that has a high $^{87}Sr/^{86}Sr$. Isotopic analyses of the Modoc HABs indicate the existence of high $^{87}Sr/^{86}Sr$ (0.7034) parental basalts in the late history of the volcano. Modoc OPOA and PA lavas have experienced AFC and mixing, but the isotopic characteristics of the HAB parent and r have varied. The high Rb contents in Burnt lava flow are puzzling and could result from mixing rhyolite with a very peculiar Rb-enriched mafic magma.

The previous discussion has revealed complexities in the interaction between AFC and magma mixing. Variability in r, differences in the end member compositions of magma mixing and changes in the characteristics of the parent HAB have occurred during the volcano's eruptive history. Changes in the AFC process, coupled with magma mixing (Fig. 5) can produce an infinite number of fractionation paths. For this reason we have not modeled fractionation of HAB to rhyolite. Rhyolites form a distinctly separate compositional group, and the absence of a recognizable variation from HAB to rhyolite prevents a quantitative treatment of the liquid line of descent to these residue compositions. In a fractionation-dominated AFC process the liquid path calculated from HAB to OPOA could be continued to rhyolite by removal of plagioclase + orthopyroxene/pigeonite + Fe − Ti oxides. Alternatively, if assimilation dominated the production of rhyolite, the characteristics of the wall rock (or stoped block) melting process would control the rhyolite composition. Fractional crystallization of HAB could produce a small amount of rhyolite, which would have isotopic characteristics identical to those of HAB parent. As r increases, the liquid line of descent changes and the volume of rhyolite attainable through fractional crystallization increases, because the general effect of assimilation is to move the bulk composition of the magmatic system further toward the end products of fractionation. The available data on silicic magmas are limited to the youngest rhyolite units, which have higher $^{87}Sr/^{86}Sr$ than any of the late Modoc HABs. The elevated $^{87}Sr/^{86}Sr$ indicates that AFC played a role in producing these compo-

sitions, but it is impossible with the available information to estimate r and the liquid line of descent to rhyolite.

The characteristics of the magma chamber(s) beneath Medicine Lake Highland control the processes that led to rhyolite. Assimilation of crust is controlled by the thermal energy that can be extracted from crystallization of the HAB (Bowen 1928, Ch. 10). Assume the wallrock is at 200° C, has its solidus at 1,000° C, and that its specific heat is 0.25 cal/g°C. To raise one gram of wallrock to the melting temperature requires 200 calories. An additional 100 cal/g must be supplied as latent heat of fusion. To melt 1 g of wallrock requires approximately 300 calories. Assuming a latent heat of crystallization of 100 cal/g for the HAB parent magma, crystallization of 3 g of basalt would produce the energy necessary to assimilate 1 gram of crustal material. A hypothetical magma body could assimilate wallrock in one of two ways. (1) Assimilation of stoped blocks could occur as part of the intrusion process that accompanies the formation of the magma chamber. For this assimilant/magma geometry small stoped blocks could be thermally engulfed by the surrounding magma and easily heated to solidus temperatures. In this case rhyolite could be produced as the end product of AFC. (2) If assimilation occurs at the boundary of the chamber, the magma must be in convective motion to raise the contact temperature above its solidus, because contact temperatures at a static magma/wallrock interface would never reach the solidus (Jaeger 1957) for the boundary conditions assumed above. In such a convecting system, the interaction of assimilated liquid and parental basalt would be influenced by convection rate and geometry. The value of r could vary, depending on the interaction between the boundary layer, where assimilation occurs, and the convecting interior of the magma chamber. If the light, buoyant boundary layer rises to the top of the chamber (McBirney 1980) and has a minimum interaction with the basalt, the r estimated from geochemical criteria would be large and in the extreme case resemble an anatectic melt. The reader is referred to McBirney (1980) for a discussion of the possible complexities in large convecting crustal magma chambers.

Liquid Densities and Magma Mixing

Stolper and Walker (1980) found that tholeiitic liquids decreased in density during crystallization of olivine as a liquidus phase and increased in density when plagioclase and pyroxene joined the crystallization sequence. Densities were calculated for the experimentally produced Medicine Lake liquids using the partial molar volumes of Bottinga and Weill (1970). Olivine+plagioclase crystallize as liquidus phases and the densities of residual liquids increase. Pyroxene joins the crystallizing assemblage and the density continues to increase (Fig. 18a) to a maximum at point A for HAB 79.35g, which is also the solidus for this composition. The Modoc BA (79.38b) has its density maximum at reaction point B, where olivine reacts out and continued plagioclase+pigeonite+oxide crystallization causes liquid density to decrease.

Densities of Medicine Lake volcanics were also calculated using the Bottinga and Weill (1970) partial molar volume data (Fig. 18b). $FeO+Fe_2O_3$ were recalculated to temperatures and oxygen fugacities of the QFM buffer (Sack et al. 1980), assuming 1,200° C for HAB, 1,100° C for andesite and 1,000° C for rhyolite and dacite. The addition of water to these lavas would lower the calculated densities. Assuming that water acts as an incompatible element, the density decrease would be greater for the evolved liquids than for the basalts, but the overall trend of decreasing density with increasing fractionation would not be altered.

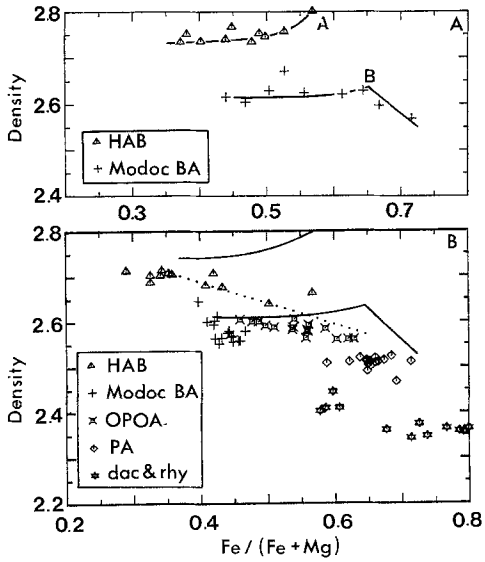

Fig. 18. A Density vs. Fe/(Fe+Mg) calculated for the HAB and Modoc BA experimental liquids. A maximum in density in the HAB data is reached at point A (Fig. 4) and the maximum density in the Modoc BAs occurs at point B. **B** Calculated densities of Medicine Lake lavas. *Solid lines* are the experimentally determined trends from (a). The *dotted line* shows the calculated variation in density for the fractional crystallization model (Table 6). Calculated density variations for an AFC model would have a steeper negative slope

The Modoc and Warner HABs form a separate trend of highest density, OPOA's and Modoc BA's are intermediate, PA's are lower at a density of ~2.5, and rhyolites and dacites are the lowest density lavas ($\rho \sim 2.37$ to 2.42). The density-composition trends for the experiments diverge from the general trend of decreasing density with increasing Fe/(Fe+Mg) formed by the lavas. Density variations for the calculated fractional crystallization model which produced OPOAs from an HAB parent (Table 6) are also shown in Fig. 18b. Density decreases steadily with increasing Fe/(Fe+Mg) and parallels the overall trend shown by the Medicine Lake lavas.

The following evolutionary model could generate the observed compositional spectrum in a single magma chamber and explain the mixed rocks. The overall trend of decreasing density from HAB to rhyolite is consistent with the magma chamber stratigraphy envisioned by McBirney (1980). Hot HAB supplied at the base of the chamber would be trapped beneath the cooler, lighter overlying layers. Assume that a magma chamber filled with parental HAB begins to cool and crystallize. At the boundaries of the chamber AFC produces a light liquid which rises to the roof to form a rhyolite cap. Within the convecting interior the magma density decreases during AFC involving olivine+plagioclase+clinopyroxene. Eventually, the residual liquid might begin to increase in density in a manner similar to the density increase shown by the 79-38b liquids as they approach point B. If another batch

of HAB is injected into the base of the chamber, it will be initially denser and trapped below the fractionated HAB. As the fresh batch of HAB cools and fractionates, its density decreases until it is less than that of the overlying fractionated liquid. Mixing of the two layers could then occur. The consequence of this mixing event could be to cool and crystallize the HAB, causing saturation with respect to a vapor phase, and resulting in boiling and eruption of a mixed lava (Eichelberger 1980; Rice 1981).

The petrographic and chemical evidence for magma mixing indicate that basalt and rhyolite were mixed to produce the Modoc BAs, and that OPOA and a rhyolite were mixed to form the PA lavas. The process discussed above only mixes evolved basaltic liquids, which differ slightly in composition, density and temperature, and does not provide a mechanism to mix the overlying rhyolite with the underlying HAB lavas. Perhaps the predicted mixing event triggers catastrophic mixing of several layers above and below those which initially mixed. In summary, the density vs. composition path followed during fractionation in calc-alkalic systems changes from decreasing to increasing density with continued fractionation in the vicinity of reaction point B. As in tholeiitic systems, which show their density maximum as A is approached, the compositions of the mixed liquids differ only slightly.

Summary and Conclusions

When Bowen laid the framework for our understanding of the process of assimilation, he argued that the major effect of assimilation was to move the magma further along in its fractionation history, and to promote crystallization of the phases already on the liquidus. He suggested that the liquid line of descent would remain essentially unaltered, and residual liquids from fractionation would remain unchanged. As we have seen in this experimental study, the complex topologies of silicate systems allow assimilation to significantly alter the liquid line of descent. As demonstrated by the HAB experiments, fractional crystallization produces an iron-enrichment trend (the Skaergaard trend) and the residual liquid composition approaches rhyolite. Assimilation of crustal material by basalt changes the bulk composition of the system so that fractionation produces calc-alkalic lavas which follow a different set of cotectics to rhyolitic residual liquids.

Processes that allow a parent basalt to follow differentiation trends characteristic of the calc-alkalic series are fractional crystallization at elevated H_2O pressure, assimilation and magma mixing. Fractional crystallization at $pH_2O >$ 1 kbar will allow liquids to evolve to compositions that can follow the calc-alkalic trend, if the liquid is moved to a shallow magma reservoir and allowed to crystallize further under low pressure conditions. Fractionation assisted by assimilation and magma mixing of basalt and rhyolite will also produce compositions that are andesitic and that can fractionate along the pigeonite and orthopyroxene saturated cotectics that are followed during calc-alkalic differentiation. Many liquid lines of descent are possible in the differentiation of parental basalt to rhyolite. Miyashiro (1974) recognized that there was not a clear distinction between calc-alkalic and tholeiitic differentiation trends and that a continuum between these two extremes existed. Fractionation, assimilation and magma mixing can exercise controls on the production of this range of trends.

Acknowledgements. This research was supported by NSF grant EAR-7919762. The authors thank Fred Frey, Julie Donnelly-Nolan, Ed Stolper and Dave Walker for interest and discussions. Ann Marie Reilly provided invaluable field assistance. Isotopic data were supported by NSF grant EAR 7803342 to S.R. Hart.

References

Albee AL, Ray L (1970) Correction factors for electron microprobe microanalysis of silicates, oxides, carbonates, phosphates and sulfates. Anal Chem 42:1408–1414

Allen JC, Boettcher AL (1978) Amphiboles in andesite and basalt: II. Stability as a function of $P-T-f_{O_2}$. Am Mineral 63:1074–1087

Anderson AT (1975) Some basaltic and andesitic gases. Rev Geophys Space Phys 13:37–55

Anderson AT (1976) Magma mixing: Petrological processes and volcanological tool. J Volcanol Geotherm Res 1:3–33

Anderson CA (1941) Volcanoes of the Medicine Lake Highland, California. Univ Calif Dept Geol Sci Bull 25:347–442

Barsky CK (1975) Geochemistry of basalts and andesites from the Medicine Lake Highland. Washington Univ, Ph D Thesis, 373 pp

Bence AE, Albee AL (1968) Empirical correction factors for the electron microanalysis of silicates and oxides. J Geol 76:382–403

Biggar GM (1972) Diopside, lithium metasilicate, and the 1968 temperature scale. Mineral Mag 38:768–770

Biggar GM (1974) Phase equilibria studies of the chilled margins of some layered intrusions. Contrib Mineral Petrol 46:159–167

Boettcher AL (1973) Volcanism and orogenic belts – the origin of andesites. Tectonophysics 17:223–240

Bottinga Y, Weill DF (1970) Densities of liquid silicate systems calculated from partial molar volumes of oxide components. Am J Sci 269:169–182

Bowen NL (1928) The Evolution of the Igneous Rocks. Princeton Univ Press Princeton, NJ, 334 pp

Briqueu L, Lancelot JR (1979) Rb–Sr systematics and crustal contamination models for calc-alkaline igneous rocks. Earth Planet Sci Lett 43:385–396

Brooks C, James DE, Hart SR (1976) Ancient lithosphere: Its role in young continental volcanism. Science 193:1086–1094

Bryan WB (1969) Materials balance in igneous rock suites. Carnegie Inst Washington Yearb 67:241–243

Cawthorn RG (1976) Some chemical controls on igneous amphibole compositions. Geochim Cosmochim Acta 40:1319–1328

Cawthorn RG, O'Hara MJ (1976) Amphibole fractionation in calc-alkaline magma genesis. Am J Sci 276:309–329

Condie KC, Hayslip DL (1975) Young bimodal volcanism at Medicine Lake volcanic center, Northern California. Geochim Cosmochim Acta 39:1163–1178

DePaolo DJ (1981) Trace element and isotopic effects of combined wallrock assimilation and fractional crystallization. Earth Planet Sci Lett 53:189–202

Donnelly-Nolan JM, Ciancanelli EV, Eichelberger JC, Fink JH, Heiken G (1981) Roadlog for field trip to Medicine Lake Highland. US Geol Surv Circ 838:141–149

Drake MJ, Weill DF (1975) Partition of Sr, Ba, Ca, Y, Eu^{2+}, Eu^{3+} and other REE between plagioclase feldspar and magmatic liquid: an experimental study. Geochim Cosmochim Acta 39:689–712

Eggler DH (1972) Water-saturated and undersaturated melting relations in a Paricutin andesite and an estimate of water content in the natural magma. Contrib Mineral Petrol 34:261–271

Eggler DH, Burnham CW (1973) Crystallization and fractionation trends in the system Andesite-H_2O-CO_2-O_2 at Pressures to 10 Kb. Geol Soc Am Bull 84:2517–2532

Eichelberger JC (1975) Origin of andesite and dacite: evidence of mixing at Glass Mountain in California and at other circum-Pacific volcanoes. Geol Soc Am Bull 86:1381–1391

Eichelberger JC (1978) Andesitic volcanism and crustal evolution. Nature 275:21–27
Eichelberger JC (1980) Vesiculation of mafic magma during replenishment of silicic magma reservoirs. Nature 288:446–450
Ewart A, Bryan WB, Gill J (1973) Mineralogy and geochemistry of the younger volcanic islands of Tonga, SW Pacific. J Petrol 14:429–465
Fenner CN (1929) The crystallization of basalts. Am J Sci 5th Ser 18:225–253
Finn C, Williams DL (1982) Gravity evidence for a shallow intrusion under the Medicine Lake Volcano, California: preliminary results. Geology (submitted)
Gill JB (1974) Role of underthrust oceanic crust in the genesis of a Fijian calc-alkaline suite. Contrib Mineral Petrol 43:29–45
Gill J (1981) Orogenic andesites and plate tectonics. Springer, New York, 390 p
Gerlach DC, Grove TL (1982) Petrology of Medicine Lake Highlands volcanics: characterization of the endmembers of magma mixing. Contrib Mineral Petrol (in press)
Green DH (1976) Experimental testing of "equilibrium" partial melting of peridotite under water-saturated, high-pressure conditions. Can Mineral 14:255–268
Green TH, Ringwood AE (1968) Genesis of the calc-alkaline igneous rock suite. Contrib Mineral Petrol 18:105–162
Grove TL (1982) Use of FePt alloys to eliminate the iron loss problem in 1 atmosphere gas mixing experiments: Theoretical and practical considerations. Contrib Mineral Petrol 78:298–304
Hart SR, Brooks C (1977) The geochemistry and evolution of early Precambrian mantle. Contrib Mineral Petrol 61:109–128
Hart SR, Davis KE (1978) Nickel partitioning between olivine and silicate melt. Earth Planet Sci Lett 40:203–219
Heiken G (1978) Plinian-type eruptions in the Medicine Lake Highland, California, and the nature of the underlying magma. J Volcanol Geotherm Res 4:375–402
Huppert HE, Sparks RSJ (1980) The fluid dynamics of a basaltic magma chamber replenished by influx of hot, dense ultrabasic magma. Contrib Mineral Petrol 75:279–289
Irvine TN (1976) Metastable liquid immiscibility and $MgO-FeO-SiO_2$ fractionation patterns in the system $Mg_2SiO_4-Fe_2SiO_4-CaAl_2Si_2O_8-KAlSi_3O_8-SiO_2$. Carnegie Inst Washington Yearb 75:597–611
Irvine TN (1977) Origin of chromitite layers in the Muskox intrusion and other stratiform intrusions: a new interpretation. Geology 5:273–277
Irving AJ (1978) A review of experimental studies of crystal/liquid trace element partitioning. Geochim Cosmochim Acta 42:743–770
James DE, Brooks C, Cuyubamba A (1976) Andean Cenozoic volcanism: magma genesis in the light of strontium isotopic composition and trace element geochemistry. Geol Soc Am Bull 87:592–600
Klerkx J, Deutsch S, Pichler H, Zeil W (1977) Strontium isotopic composition and trace element data bearing on the original Cenozoic volcanic rocks of the central and southern Andes. J Volcanol Geotherm Res 2:49–71
Kuno H (1936) Petrological notes on some pyroxene andesites from Hakone volcano, with special reference to some types with pigeonite phenocrysts. Jpn J Geol Geogr 13:107–140
Kuno H (1950) Petrology of Hakone volcano and the adjacent areas, Japan. Geol Soc Am Bull 61:957–1019
Kuno H (1965) Fractionation trends of basalt magmas in lava flows. J Petrol 6:302–321
Kushiro I (1972a) Effect of water on the composition of magmas formed at high pressures. J Petrol 13:311–334
Kushiro I (1972b) Determination of liquidus relations in synthetic silicate systems with electron probe analysis: the system forsterite-diopside-silica at 1 atmosphere. Am Mineral 57:1260–1271
Larsen ES, Irving J, Bonyer FA (1938) Petrologic results of a study of the minerals from the Tertiary volcanic rocks of the San Juan region, Colorado. Am Mineral 23:227–257, 417–429
Longhi J, Boudreau AE (1979) Pyroxene liquidus fields in basaltic liquids at low pressure (abstr). Lunar Planet Sci 10:739–741 10:739–741
Longhi J, Boudreau AE (1980) The orthoenstatite liquidus field in the system forsterite-diopside-silica at one atmosphere. Am Mineral 65:563–573
MacBirney AR (1980) Mixing and unmixing of magmas. J Volcanol Geotherm Res 7:357–371
Marsh BD, Kantha LH (1978) On the heat and mass transfer from an ascending magma. Earth Planet Sci Lett 39:435–443
Mertzman SA (1977a) Recent volcanism at Schonchin and Cinder Buttes, Northern California. Contrib Mineral Petrol 61:231–243
Mertzman SA (1977b) The petrology and geochemistry of Medicine Lake Volcano, California. Contrib Mineral Petrol 62:221–247
Mertzman SA Jr (1978) A tschermakite-bearing high-alumina olivine tholeiite from the Southern Cascades, California. Contrib Mineral Petrol 67:261–265
Mertzman SA (1979) Strontium isotope geochemistry of a low-potassium olivine tholeiite and two basalt-pyroxene andesite magma series from the Medicine Lake Highland, California. Contrib Mineral Petrol 70:81–88
Mertzman SA, Williams RJ (1981) Genesis of recent silicic magmatism in the Medicine Lake Highland, California: evidence from cognate inclusions found at Little Glass Mountain. Geochim Cosmochim Acta 45:1463–1478
Miyashiro A (1974) Volcanic rock series in island arcs and active continental margins. Am J Sci 274:321–355
Mysen BO, Kushiro I, Nicholls IA, Ringwood AE (1974) A possible mantle origin for andesite magmas: discussion and replies. Earth Planet Sci Lett 21:221–229
Nicholls IA, Ringwood AE (1972) Production of silica-saturated magmas in island arcs. Earth Planet Sci Lett 17:243–246
Nicholls IA, Ringwood AE (1973) Effect of water on olivine stability in tholeiite and the production of silica-saturated magmas in the island-arc environment. J Geol 81:285–300
O'Hara MJ (1968) The bearing of phase equilibria studies in synthetic and natural systems on the origin and evolution of basic and ultrabasic rocks. Earth Sci Rev 4:60–133
O'Hara MJ (1977) Geochemical evolution during fractional crystallization of a periodically refilled magma chamber. Nature 266:503–507
Osborn EF (1959) Role of oxygen pressure in the crystallization and differentiation of basaltic magma. Am J Sci 257:609–647
Peterman ZE, Carmichael ISE, Smith AL (1970) Sr^{87}/Sr^{86} ratios of Quaternary lavas of the Cascade range, Northern California. Geol Soc Am Bull 81:311–318
Peterman ZE, Hedge CE, Coleman RG, Shavely PD Jr (1967) $^{87}Sr/^{86}Sr$ ratios in some eugeosynclinal sedimentary rocks and their bearing on the origin of granitic magma in orogenic belts. Earth Planet Sci Lett 2:433–439
Pettijohn FJ (1975) Sedimentary rocks, third edition. Harper and Row, New York, 628 p
Rice A (1981) Convective Fractionation: A mechanism to provide cryptic zoning (macrosegregation), layering, crescumulates, banded tuffs and explosive volcanism in igneous provinces. J Geophys Res 86:405–417
Ringwood AE (1974) The petrological evolution of island arc systems. J Geol Soc London 130:183–204
Sack RO, Carmichael ISE, Rivers M, Ghiorso MS (1980) Ferric-ferrous equilibria in natural silicate liquids at 1 bar. Contrib Mineral Petrol 75:369–376
Smith AL, Carmichael ISE (1968) Quaternary lavas from the southern Cascades, western USA. Contrib Mineral Petrol 19:212–238
Sparks RSJ, Meyer P, Sigurdsson H (1980) Density variation amongst mid-ocean ridge basalts: implications for magma mixing and the scarcity of primitive lavas. Earth Planet Sci Lett 46:419–430
Stolper E (1980) A phase diagram for mid-ocean ridge basalts:

Preliminary results and implications for petrogenesis. Contrib Mineral Petrol 74:13–27
Stolper E, Walker D (1980) Melt density and the average composition of basalt. Contrib Mineral Petrol 74:7–12
Taylor HP Jr (1980) The effects of assimilation of country rocks by magmas on $^{18}O/^{16}O$ and $^{87}Sr/^{86}Sr$ systematics in igneous rocks. Earth Planet Sci Lett 47:243–254
Turner JS, Chen CF (1974) Two-dimensional effects in double-diffusive convection. J Fluid Mech 63:577–592
Wager LR, Deer WA (1939) The petrology of the Skaergaard intrusion, Kangerdlassuaq, East Greenland. Meddel öm Grönland 105, no 4, 352 p
Walker D, Shibata T, DeLong SF (1979) Abyssal tholeiites from the Oceanographer Fracture Zone II, Phase equilibria and mixing. Contrib Mineral Petrol 70:111–125
White CM, MacBirney AR (1978) Some quantitative aspects of orogenic volcanism in the Oregon Cascades. Geol Soc Am Mem 152:369–388
Wilcox RE (1954) Petrology of Paricutin Volcano, Mexico. US Geol Surv Bull 965-C:281–353
Yoder HS Jr, Tilley CE (1962) Origin of basalt magmas: An experimental study of natural and synthetic rock systems. J Petrol 3:342–532

Received October 9, 1981; Accepted in revised form June 14, 1982